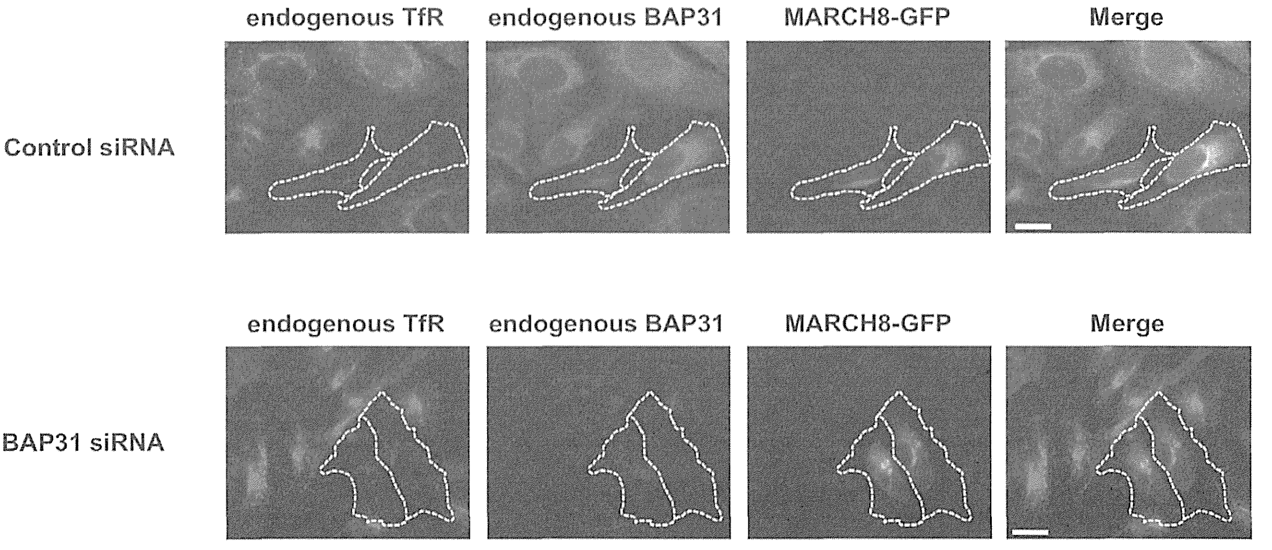

Fig. S4. Effect of the siRNA-mediated knockdown of BAP31 on the downregulation of TfR induced by MARCH8. HeLa cells transfected with siRNA for either control or BAP31 (Mission RNA; Sigma) were cultured for 48 h. The cells were transfected with the plasmid encoding WT MARCH8-GFP, cultured for another 24 h, and processed for IF with anti-BAP31 (blue) and anti-TfR (red) antibodies. The cells expressing MARCH8-GFP (green) are indicated by the yellow dotted lines. Scale bar: 20 μm.

frontiers in
MICROBIOLOGY

ORIGINAL RESEARCH ARTICLE
published: 17 December 2013
doi: 10.3389/fmicb.2013.00377

Transgenic expression of the human LEDGF/p75 gene relieves the species barrier against HIV-1 infection in mouse cells

Takuya Tada[1,2,3,4], *Motohiko Kadoki*[1,5], *Yang Liu*[1,6], *Kenzo Tokunaga*[4]* and *Yoichiro Iwakura*[1,2,3,5]*

[1] Center for Experimental Medicine and System Biology, Institute of Medical Science, University of Tokyo, Tokyo, Japan
[2] Department of Biophysics and Biochemistry, Graduate School of Science, University of Tokyo, Tokyo, Japan
[3] Core Research for Evolutional Science and Technology, Japan Science and Technology Agency, Saitama, Japan
[4] Department of Pathology, National Institute of Infectious Diseases, Tokyo, Japan
[5] Research Institute for Biomedical Sciences, Tokyo University of Science, Chiba, Japan
[6] Stem Cell Research Center, Shanghai Jiao Tong University School of Medicine Renji Hospital, Shanghai, China

Edited by:
Akio Adachi, The University of Tokushima Graduate School, Japan

Reviewed by:
Akio Adachi, The University of Tokushima Graduate School, Japan
Masako Nomaguchi, The University of Tokushima Graduate School, Japan

***Correspondence:**
Kenzo Tokunaga, Department of Pathology, National Institute of Infectious Diseases, 1-23-1 Toyama, Shinjuku-ku, Tokyo 162-8640, Japan
e-mail: tokunaga@nih.go.jp;
Yoichiro Iwakura, Center for Animal Disease Models, Research Institute for Biomedical Sciences, Tokyo University of Science, 2669 Yamazaki, Noda, Chiba 278-0022, Japan
e-mail: iwakura@rs.tus.ac.jp

Attempts to create mouse models for AIDS have been hampered by species barriers in HIV-1 infection. We previously showed that the nuclear accumulation of HIV-1 preintegration complex (PIC) was suppressed in mouse cells. Lens epithelium-derived growth factor (LEDGF/p75) is a host factor identified as a binding partner of integrase (IN), and has been suggested to be involved in promoting viral integration by tethering PIC to the chromatin, which are observed as nuclear accumulation of IN by LEDGF/p75. Therefore, we here hypothesized that this host factor might act as one of the species-specific barriers in mouse cells. We generated transgenic (Tg) mice that constitutively express human (h) LEDGF/p75. The GFP-fused IN was efficiently accumulated into the nucleus of hLEDGF/p75 expressing Tg mouse embryonic fibroblast (MEF) cells in contrast to the control MEF cells. Importantly, hLEDGF/p75 Tg MEF cells were significantly more susceptible to HIV-1 infection. These results suggest that LEDGF/p75 is one of the host factors that constitute species barrier against HIV-1 in mouse cells.

Keywords: HIV-1, LEDGF/p75, IN, transgenic mouse, species barrier

INTRODUCTION

The number of patients with HIV/AIDS has been increasing throughout the world. In order to study AIDS pathogenesis and to evaluate antiviral drugs and vaccines, animal models for HIV-1 infection need to be established. A mouse model has been considered as one of such candidates because of the availability of inbred and gene-manipulated strains. As a matter of fact, mice are non-permissive for HIV-1 infection because of the species barriers against both the early, and late phases of HIV-1 infection (van Maanen and Sutton, 2003), although the precise mechanisms for the non-permissiveness remain unclear. The finding that the heterokaryons created between human and mouse cells were susceptible to HIV-1 infection (Dragic et al., 1992; Mariani et al., 2001) suggested that mouse cells lack some human-specific cofactors that can support HIV-1 replication.

A number of factors in host cells have been implicated to be involved in the early and late phases of HIV-1 infection; e.g., CD4 as the major receptor for HIV-1 entry (Maddon et al., 1985; Lores et al., 1992), chemokine receptors as coreceptors (Berson et al., 1996; Feng et al., 1996) and cyclin T1 (CycT1) for the efficient viral transcription through binding to HIV-1 Tat (Bieniasz et al., 1998; Wei et al., 1998). However, several Tg mice lines that express human versions of CD4, either CXCR4 (hCD4/hCXCR4/hCycT1 Tg) or CCR5 (hCD4/hCCR5/hCycT1 Tg), and CycT1 did not efficiently support HIV-1 replication despite HIV-1 entry and reverse transcription proceeded normally (Browning et al., 1997; Sawada et al., 1998; Mariani et al., 2000). On the other hand, Tg mice carrying the *pol* gene-deleted HIV-1 proviral genome (HIV-Tg), which we previously generated, were able to not only express all viral mRNA species, including unspliced, singly spliced, and multiply spliced mRNAs, but also produce high levels of gag p24 antigen, after treatment with bacterial lipopolysaccharides (LPS) (Iwakura et al., 1992). Taken together, these results indicate that once the viral genome is efficiently integrated into the host chromosome, viral genes are expressed normally, and that unknown species barriers in mice are still present in the early phase of HIV-1 infection.

HIV-1 preintegration complex (PIC) is composed of newly synthesized viral cDNA and several host and viral proteins, the latter of which include integrase (IN), reverse transcriptase (RT), matrix (MA) and Vpr. The PIC is actively accumulated into the nucleus. We previously showed that the nuclear accumulation of GFP-fused IN (GFP-IN) was significantly reduced in mouse cells than in human cells (Tsurutani et al., 2007), suggesting that inefficient PIC nuclear accumulation in mouse cells might be attributed to the inability of IN to interact with host factors. Lens epithelium-derived growth factor (LEDGF) could be one of such candidates in that it can associate with IN and mediate HIV-1 nuclear accumulation and integration into the chromosome in human cells (Maertens et al., 2003). LEDGF is translated into two proteins, p75 and p52, as a result of alternative splicing (Ge et al., 1998a). LEDGF/p75, but not p52, can associate with IN through its IN-binding domain (IBD; Ge et al., 1998b). Moreover, IN and LEDGF/p75 co-localize in the nucleus of human cells, and recombinant LEDGF/p75 robustly enhances strand transfer activity of IN *in vitro* (Singh et al., 1999). It was also shown that RNAi-mediated knockdown of endogenous LEDGF/p75 abolished IN nuclear accumulation, HIV-1 integration and HIV-1 production (Maertens et al., 2003; Llano et al., 2004b; Ciuffi et al., 2005). LEDGF/p75 is also known as a critical factor for the selection of integration sites such as promoter regions and CpG islands. Thus, LEDGF/p75 has been suggested to be one of important host factors at the PIC nuclear accumulation and integration steps (Bukrinsky, 2004; Llano et al., 2004a, 2006a; Emiliani et al., 2005; Maillot et al., 2013).

In this study, we first created expression plasmids encoding human and mouse LEDGF/p75 (hLEDGF/p75 or mLEDGF/p75, respectively) to compare their ability to support HIV-1 infection in mouse embryonic fibroblast (MEF) cells, and found that the expression of hLEDGF/p75 rendered MEF cells more sensitive to HIV-1 infection than that of mLEDGF/p75. Moreover, we generated hLEDGF/p75 transgenic (hLEDGF/p75 Tg) mice and examined if the expression of hLEDGF/p75 could relieve the species barrier of HIV-1 infection in mouse cells. Transgenic expression of hLEDGF/p75 enhanced IN accumulation in the nucleus and HIV-1 infection in mouse cells, suggesting that LEDGF/p75 is one of the host factors that may determine a species barrier against HIV-1 in mouse cells. We therefore conclude that the transgenic introduction of hLEDGF/p75 would be helpful to generate a small animal model that could be more permissive to HIV-1 infection.

MATERIALS AND METHODS

CELLS

HeLa, 293T, and MT4 cells were obtained from ATCC (Rockville, USA), the RIKEN Cell Bank (Ibaraki, Japan), and the Health Science Research Resources Bank (Osaka, Japan), respectively. MEF cells from LEDGF/p75 Knockout mice were kindly provided by A. Engelman (Shun et al., 2007). HeLa, 293T, and MEF cells were maintained in Dulbecco's modified Eagle's medium (DMEM; Life Technologies, NY, USA) supplemented with 10% fetal bovine serum (FBS). MT4 cells were maintained in RPMI 1640 medium (Life Technologies, NY, USA) supplemented with 10% FBS.

PLASMIDS

Env-deficient HIV-1 proviral indicator construct pNL-Luc-E-R+, a vesicular stomatitis virus G (VSV-G)-expressing plasmid pHIT/G, and an HIV-1 NL-Env expression plasmid pNLnΔBS (Tokunaga et al., 1998) were described previously (Fouchier et al., 1997; Tokunaga et al., 2001). The expression vector for a codon-optimized HIV-1 IN fused N-terminally to GFP (GFP-IN) was previously constructed (Tsurutani et al., 2007). The hLEDGF/p75 transgene was constructed as follows. hLEDGF/p75 cDNA was obtained from HeLa cells using SuperScript First-Strand Synthesis System (Invitrogen, CA, USA). A 1.6 kb hLEDGF/p75 fragment was amplified by PCR with KOD-Plus- (TOYOBO, Osaka, Japan). The primer pairs used to amplify hLEDGF/p75 fragments were as follows: forward primer 5′-ACG AAT TCG CCA CCA TGA CTC GCG ATT TCA AAC CTG GAG ACC-3′, reverse primer 5′-CCG AAT TCT CAG TTA TCT AGT GTA GAA TCC TTC AGA GAT ATT TCA G-3′, that have *EcoR*I site, Kozak sequence respectively. PCR product was digested with *EcoR*I and inserted into pCAGGS mammalian expression vector (Niwa et al., 1991). Similarly, C-terminally HA-tagged versions of these plasmids were created by using pCAGGS-3HA expression vector (Iwabu et al., 2009). To generate CD4/CXCR4 expression plasmid, CD4, CXCR4, and ECMV IRES were PCR-amplified from pNL-CD4, pNL-CXCR4 (Tokunaga et al., 2001), and pIRESpuro2 (Clontech, CA, USA), and then digested with *Kpn*I/*Xho*I, *Xho*I/*Not*I, and *Not*I, respectively. Digested fragments were inserted into pCAGGS and the resultant expression plasmid was designated pCa-CD4/CXCR4.

TRANSFECTIONS AND PROTEIN ANALYSES

5×10^5 293T cells were transfected with 0.5 μg of either hLEDGF/p75 or mLEDGF/p75 expression plasmid by using FuGENE6 transfection reagent (Promega, Wisconsin, USA), and grown for 48 h. Cell extracts were subjected to gel electrophoresis and then transferred to a nitrocellulose membrane. The membranes were probed with an anti-HA antibody (BD biosciences, NJ, USA). Reacted proteins were visualized by chemiluminescence using an ECL Western blotting detection system (GE Healthcare, Little Chalfont, UK) and monitored using a LAS-3000 imaging system (FujiFilm, Tokyo, Japan).

INFECTION OF MEF CELLS TRANSIENTLY EXPRESSING LEDGF/p75 WITH HIV-1 REPORTER VIRUSES

2.5×10^5 MEF cells derived from LEDGF/p75 knockout mice were cotransfected with 0.5 μg of either hLEDGF/p75 or mLEDGF/p75 expression plasmid, 0.5 μg of pCa-CD4/CXCR4, and 5 ng of phRL-TK Renilla luciferase expression plasmid (Promega) by using Lipofectamine with Plus reagents (Life Technologies) and grown for 48 h. Infection experiments were performed as described below. Viruses were prepared by cotransfecting 293T cells with 1 μg of pNL-Luc-E-R+, 0.5 μg of pNLnΔBS, and 0.5 μg of an empty plasmid by using FuGENE6. After 48 h, the supernatants were treated with 37.5 units/ml DNase I (Roche Applied Science, MD, USA) for 37°C for 30 min and then harvested, and the amount of p24 antigen was measured by using an HIV-1 p24-antigen capture enzyme-linked immunosorbent assay (ELISA) (Advanced BioScience Laboratories, CA, USA). 1×10^4 MEF cells transiently expressing either hLEDGF/p75 or mLEDGF/p75 were infected with 1 ng of p24 antigen of HIV-1 reporter viruses. At 48 h after infection, cells were lysed with Passive Lysis Buffer (Promega). Cell lysates were subjected to the luciferase assay using the Dual Luciferase Reporter Assay Systems (Promega). Luciferase activity was measured by Centro LB 960 Microplate Luminometer (Berthold Technologies, Bad Wildbad, Germany). Values were normalized by Renilla luciferase activity.

GENERATION OF hLEDGF/p75 Tg MICE

The hLEDGF/p75 trangene was digested with *BamHI-HindIII*, purified from agarose gel with GeneClean Kit (MP-Biomedicals, CA, USA) and adjusted to a final concentration of 5×10^5 copies/μl (2.13 ng/μl). Purified fragments were injected into the male pronuclei of fertilized mouse embryos (C3H/HeN; CLEA Japan Inc, Tokyo, Japan). Mice were kept under specific-pathogen-free conditions in an environmentally controlled clean room at the Center for Experimental Medicine and Systems Biology, the Institute of Medical Science, the University of Tokyo. All experiments were done according to the ethical guidelines for animal experimentation, which was approved by the Institutional Review Board of the Institute of Medical Science, the University of Tokyo.

SOUTHERN BLOT HYBRIDIZATION

Southern blot analyses were carried out as previously described (Smith and Murphy, 1993). Genomic DNA (10 μg) extracted from the mouse tails was digested with *PstI*. Digested DNA was electrophoresed and blotted onto a membrane. Membrane was hybridized with ^{32}P labeled probe. To detect hLEDGF/p75, an *EcoRI-PstI* (540 bp) fragment from pCAGGS was used as a β-globin probe. The autoradiograms were developed and the band intensity was quantified by a BAS 2000 Bio-Image analyzer (FujiFilm, Tokyo, Japan). Alpha-fetoprotein (AFP) was used as an internal control.

NORTHERN BLOT HYBRIDIZATION

Total RNA from the thymus, spleen, lymph nodes and thioglycolate (TGC)-elicited macrophages of hLEDGF/p75 Tg mice was prepared by the acid guanidium thiocyanate phenol chloroform method (Chomczynski and Sacchi, 1987). In order to obtain macrophages, mice were injected intraperitoneally with 2 ml of 4% TGC (Difco Laboratories, MI, USA). Three days later, peritoneal exudate cells were collected (Saijo et al., 2007). Northern blot analyses were carried out as previously described (Yasuda et al., 2001). hLEDGF/p75 probe (1.6 kb) was generated by PCR with KOD-Plus- by using the following primers: forward primer; 5′-ACG AAT TCG CCA CCA TGA CTC GCG ATT TCA AAC CTG GAG ACC-3′, reverse primer; 5′-CCG AAT TCT CAG TTA TCT AGT GTA GAA TCC TTC AGA GAT ATT TCA G-3′. The autoradiograms were developed, and the radioactivity of each the bands was quantified with the BAS 2000 Bio-Image analyzer (FujiFilm).

REAL-TIME RT-PCR

Total RNA from MEF cells was extracted using ReliaPrep RNA Cell Miniprep System (Promega) according to the manufacturer's instructions. Real-time RT-PCR was performed using One Step SYBR PrimeScript RT-PCR Kit (Takara, Shiga, Japan) with the ABI PRISM 7900HT Sequence Detection System. hLEDGF/p75 mRNA was detected by using the following primers: forward primer; 5′-GAG AAA CAT CAA TGG ATT CTC GAC-3′ and reverse primer; 5′-CTC AAT GCA TCT GTT CAC ATC AAG-3′. GAPDH was detected by using the following primers: forward primer; 5′-GAT GCT GGC GCT GAG TAC G-3′ and reverse primer; 5′-GCA GAG ATG ATG ACC CTT TTG-3′. Levels of hLEDGF/p75 mRNA were normalized with those of GAPDH mRNA.

PREPARATION OF MEF CELLS EXPRESSING hLEDGF/p75

Mouse embryonic fibroblast cells from hLEDGF/p75 Tg and wild-type (WT) mice were prepared as follows. Fetuses were harvested at 13.5 days of gestation. Embryonic internal organs were removed from the abdominal cavity using dissecting forceps. The embryos were transferred to a 10 cm dish containing 10 ml trypsin/EDTA solution and incubated 20 min at 37°C. After trypsinization, cells were washed and cultured in DMEM. Cell extracts were subjected to gel electrophoresis and then transferred to a nitrocellulose membrane. The membranes were probed with an anti-hLEDGF/p75 antibody (BD biosciences, NJ, USA). Reacted proteins were visualized by chemiluminescence using an ECL Western blotting detection system and monitored using a LAS-3000 imaging system.

FLUORESCENCE MICROSCOPY

One day prior to transfection, 2×10^5 HeLa, and MEF cells were plated in 8 well culture slides (Nalgene Nunc International, NY, USA) and transfected with 0.8 μg of DNA (GFP-IN) per well using Lipofectamine 2000 (Invitrogen). After 6 h, medium was replaced with fresh culture medium. Forty eight hours post-transfection, cells were washed once in PBS and fixed with acetone for 5 min. After washing with PBS, 1 μg/ml of Hoechst suspended in PBS was added. After 10 min incubation, cells were covered by a coverslip. Confocal microscopy was performed with a Nikon Optiphot-2 fluorescence microscope with a Bio-Rad MRC 1024 laser confocal imaging system (Nikon, Tokyo, Japan).

INFECTION OF hLEDGF/p75 Tg MEF CELLS WITH VSV-G-PSEUDOTYPED HIV-1 REPORTER VIRUSES

The VSV-G pseudotyped NL4-3-Luc viruses were produced by cotransfecting 293T cells with 1.9 μg of pNL-Luc-E-R+ and 0.1 μg of pHIT/G by using FuGENE6. After 48 h, the supernatants were treated with DNase I for 37°C for 30 min and then harvested, and the amount of p24 antigen was measured by using an HIV-1 p24-antigen capture ELISA. 1×10^4 hLEDGF/p75 Tg MEF cells (No. 089, 110, and 143) were infected with 200 pg of p24 antigen of VSV-G-pseudotyped HIV-1 reporter viruses. At 48 h after infection, cells were lysed with Passive Lysis Buffer and subjected to the luciferase assay. Luciferase activity was measured by Centro LB 960 Microplate Luminometer.

RESULTS

FUNCTIONAL DIFFERENCE BETWEEN HUMAN AND MURINE LEDGF/p75 PROTEINS

We previously showed that the nuclear accumulation of PIC was blocked in mouse cells (Tsurutani et al., 2007), suggesting that mLEDGF/p75 might be defective at this step. To test this hypothesis, we created HA-tagged hLEDGF/p75 and mLEDGF/p75 expression plasmids. Protein expressions in the cells transfected with each plasmid were confirmed by immunoblotting using anti-HA antibodies (**Figure 1A**). We cotransfected MEF cells derived from LEDGF/p75 knockout mice with either hLEDGF/p75 or mLEDGF/p75, together with CD4/CXCR4 expression plasmid. We then examined the efficiency of HIV-1 infection by using MEF cells transiently expressing hLEDGF/p75 or mLEDGF/p75. We

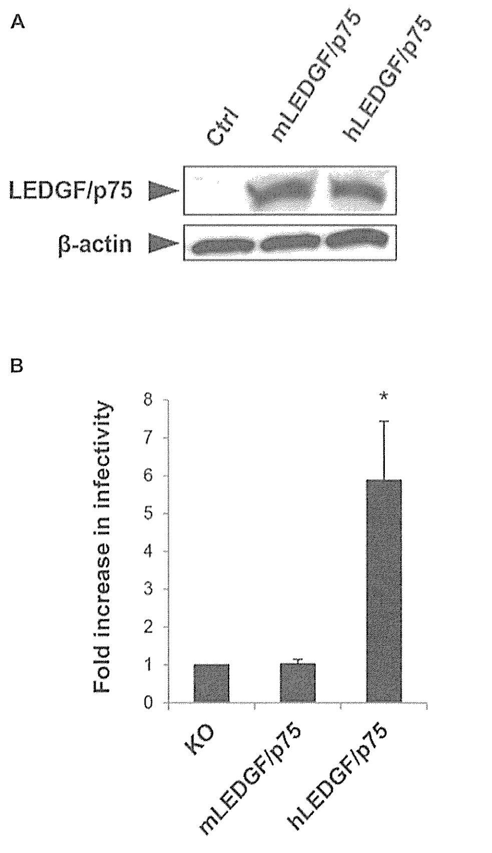

FIGURE 1 | Comparison of hLEDGF/p75 and mLEDGF/p75 in the ability to support HIV-1 infection. (A) Detection of hLEDGF/p75 and mLEDGF/p75 proteins. 293T cells were transfected with either hLEDGF/p75 or mLEDGF/p75 expression plasmid and grown for 48 h. Western blot was performed to detect LEDGF/p75 proteins by using an anti-HA antibody. β-actin was used as an internal control. **(B)** HIV-1 infectivity in cells expressing different LEDGF/p75 proteins. MEF cells derived from LEDGF/p75 knockout (KO) mice were cotransfected with either hLEDGF/p75 or mLEDGF/p75 expression plasmid, pCa-CD4/CXCR4, and phRL-TK Renilla luciferase expression plasmids, and grown for 48 h. MEF cells transiently expressing either hLEDGF/p75 or mLEDGF/p75 were infected with HIV-1 reporter viruses. At 48 h after infection, cells were subjected to the luciferase assay. Values were normalized with Renilla luciferase activity. $^*P < 0.01$ (*t*-test).

found that infection was more efficient in MEF cells expressing hLEDGF/p75 than those expressing mLEDGF/p75 (**Figure 1B**). These results suggest that hLEDGF/p75 expression renders MEF cells more susceptible to HIV-1 infection.

GENERATION OF TRANSGENIC MICE CARRYING THE hLEDGF/p75

We generated Tg mice carrying the hLEDGF/p75 to examine whether the host factor would be able to confer HIV-1 susceptibility to the animals. To obtain Tg mice expressing high levels of hLEDGF/p75 in multiple tissues, a transgene consisting of the cytomegalovirus immediate-early enhancer/chicken β-actin promoter, the hLEDGF/p75 cDNA and rabbit β-globin poly A, was constructed (**Figure 2A**). Transgenic founders were obtained by microinjecting the transgene into the pronuclei of fertilized

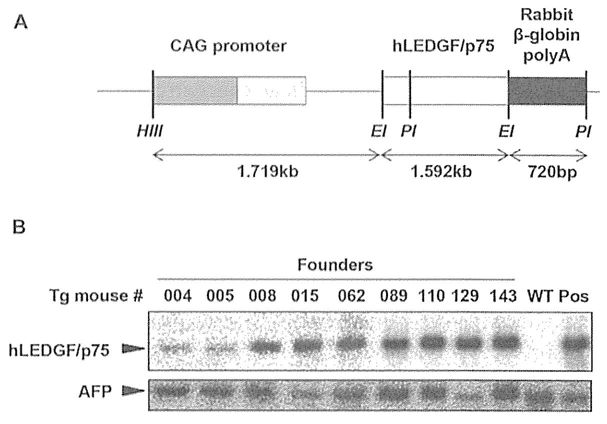

FIGURE 2 | Generation of hLEDGF/p75 Tg mice. (A) Construction of the transgene. hLEDGF/p75 gene (white box) was ligated downstream of the CMV-immediate-early enhancer/chicken β-actin promoter (CAG) promoter. Restriction enzyme sites are indicated as follows: *Hin*dIII (HIII), *Eco*RI (EI) and *Pst*I (PI). **(B)** Detection of the transgene in hLEDGF/p75 Tg mice by Southern blot hybridization analysis. Cellular DNA (10 μg) was extracted from the mouse tails, digested with *PstI*, and was electrophoresed in an agarose gel. β-globin poly A was used as a probe (black box). Cellular DNA from WT mouse was used as a negative control (WT), and WT DNA containing pCAGGS-hLEDGF/p75 plasmid copies was used as a positive control (Pos). Alpha-fetoprotein (AFP) was used as an internal control. The sizes expected for hLEDGF/p75 and AFP are indicated by arrowheads.

embryos from WT parents (C3H/HeN). Southern blot hybridization was carried out to detect the transgene by using a probe specific for β-globin polyA. Out of 165 offspring, we obtained 9 transgenic founder mice in which the hLEDGF/p75 transgene was integrated (**Figure 2B**).

hLEDGF/p75 TRANSGENE EXPRESSION IN hLEDGF/p75 Tg MICE

In order to analyze the expression of hLEDGF/p75 mRNA in hLEDGF/p75 Tg F1 mice, Northern blot hybridization was performed by using total RNAs purified from thymus, spleen, lymph-nodes, and TGC-elicited macrophages. As shown in **Figure 3A**, 1.7 kb bands were detected in hLEDGF/p75 Tg mice, while the endogenous 2.1 kb bands were detected in HeLa and MT4 cells. hLEDGF/p75 mRNA from line No. 089 Tg mouse was detected in all the tissues, in which levels of hLEDGF/p75 expression was similar to those in HeLa or MT4 cells. The mRNA was also present in the thymus and spleen derived from the line No. 110 Tg mouse, in the thymus, spleen and lymph-nodes of the line No. 143 Tg mouse (**Figures 3A,B**). Either the line No. 004, 005, 008, 015, and 062 Tg mice or the line No. 129 Tg mice expressed only in the thymus or lymph-nodes, respectively (data not shown). For further studies, we thus selected 3 lines (line No. 089, 110, and 143 Tg mice) expressing relatively high hLEDGF/p75 mRNA in the thymus, spleen and lymph nodes.

ESTABLISHMENT OF MEF CELLS DERIVED FROM hLEDGF/p75 Tg MICE

To investigate whether hLEDGF/p75 promotes IN nuclear accumulation, we examined the subcellular localization of IN in hLEDGF/p75 Tg mouse cells. We generated MEF cells from hLEDGF/p75 Tg mice and the expression of hLEDGF/p75 was

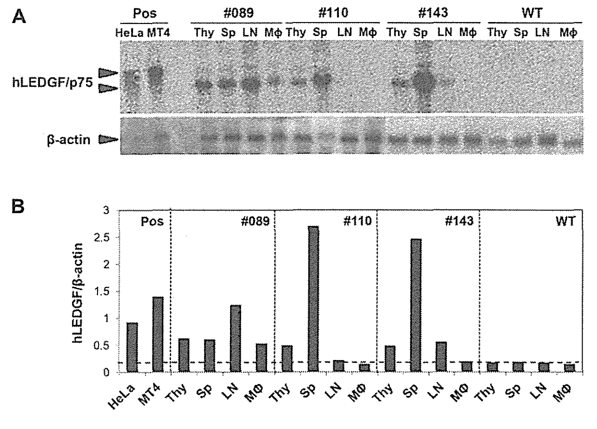

FIGURE 3 | hLEDGF/p75 expression in Tg mice. (A) Total RNA was extracted from the thymus (Thy), spleen (Sp), lymph-nodes (LN), and TGC-elicited macrophages from hLEDGF/p75 Tg mice. Northern blot hybridization was carried out using 10 μg of RNA prepared from tissues. hLEDGF/p75 cDNA was used as a probe, and β-actin was used as an internal control. RNA from the WT mouse and from HeLa and MT4 cells were used as a negative control (WT), and as positive controls (Pos), respectively. The sizes expected for hLEDGF/p75 and β-actin are indicated by arrowheads. **(B)** The band intensity in **(A)** was measured with a BAS 2000 Bio-Image analyzer. Expression levels of hLEDGF/p75 relative to those of β-actin are shown for each transgenic line. The threshold is indicated by a horizontal dotted line.

examined. As shown in **Figure 4A**, MEF cells from hLEDGF/p75 Tg mice were prepared from mice fetuses. Tg mice were mated with WT, and fetuses were harvested at 13.5 days of gestation and removed embryonic internal organs from the abdominal cavity. The embryos were dissociated and trypsinized to produce single-cell suspensions. After expansion, we confirmed that hLEDGF/p75 mRNA (**Figure 4B**) as well as hLEDGF/p75 protein (**Figure 4C**) was detected in MEF cells from the line No. 089, 110, and 143 Tg mice.

ENHANCED NUCLEAR ACCUMULATION OF GFP-IN IN MEF CELLS FROM hLEDGF/p75 Tg MICE

HeLa cells, and MEF cells derived from either WT or hLEDGF/p75 Tg mice (line No. 089, 110, and 143) were transfected with a plasmid expressing codon-optimized IN that was N-terminally fused to GFP, and the subcellular localization was examined by fluorescence and confocal microscopy. As shown in **Figure 5A**, we observed the accumulation of GFP-IN in the nucleus of hLEDGF/p75 Tg-derived MEF cells, making a clear contrast to those from WT mice. To quantitatively evaluate the efficiency of nuclear accumulation of GFP-IN, we classified the cells as follows; (N) the fluorescence of GFP-IN is higher in the nucleus than in the cytoplasm; (N/C) the fluorescence of GFP-IN in the nucleus is similar to the cytoplasm; and (C) the fluorescence of GFP-IN is higher in the cytoplasm than in the nucleus (**Figure 5B**). As expected, GFP-IN preferentially localized mainly into the nucleus in HeLa cells (N: 93.1%), while GFP-IN did not localize exclusively in the nucleus in WT MEF cells (N: 14.2%) but mainly in both the cytoplasm and the nucleus in WT MEF cells (N/C: 56.7%). In contrast, GFP-IN significantly accumulated in the nucleus in MEF cells from line No. 089, 110, and 143 Tg mice (N: 70.8, 49.5, and 65.7, respectively; **Figure 5C**). These data suggest that hLEDGF/p75 enhances IN accumulation into the nucleus of

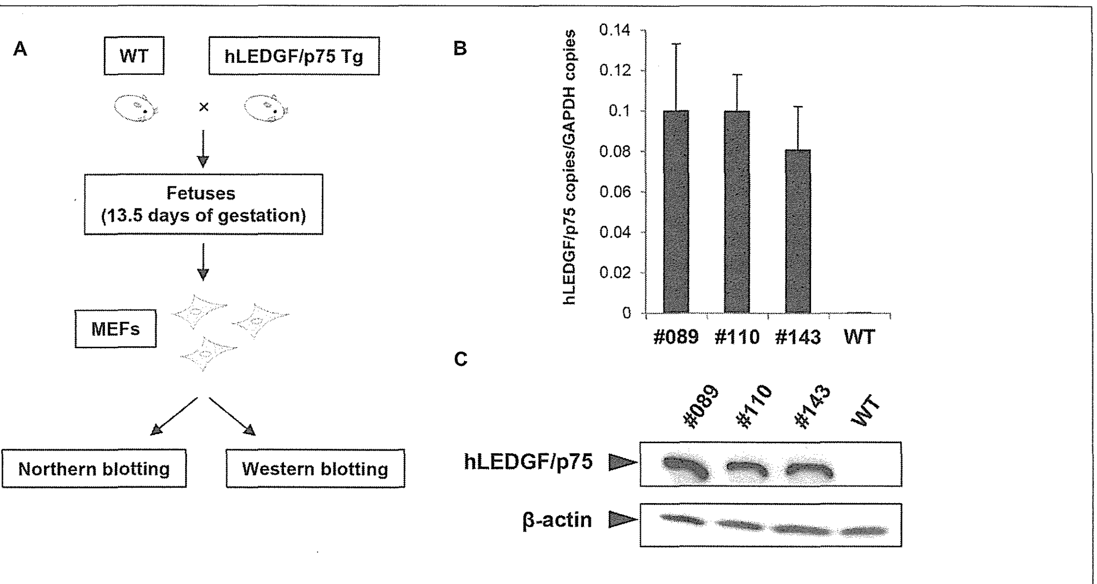

FIGURE 4 | Preparation of MEF cells and hLEDGF/p75 expression in MEF cells. (A) MEF cells from hLEDGF/p75 Tg and WT mice were prepared from mice fetuses. Mice were mated with WT mice, and the resulting fetuses were harvested at 13.5 days of gestation. Embryonic internal organs were removed from the abdominal cavity. The embryos were dissociated and trypsinized to produce single-cell suspensions. After expansion, the expression of hLEDGF/p75 in MEF cells was analyzed. **(B)** Real-time RT-PCR was performed to evaluate the hLEDGF/p75 mRNA expression in hLEDGF/p75 Tg MEF cells by using hLEDGF/p75 specific primers. The copy numbers were normalized with that of GAPDH. **(C)** Western blotting was carried out using proteins from Tg and WT MEF cells. An anti-hLEDGF/p75 antibody was used to detect the protein, and β-actin was detected as an internal control.

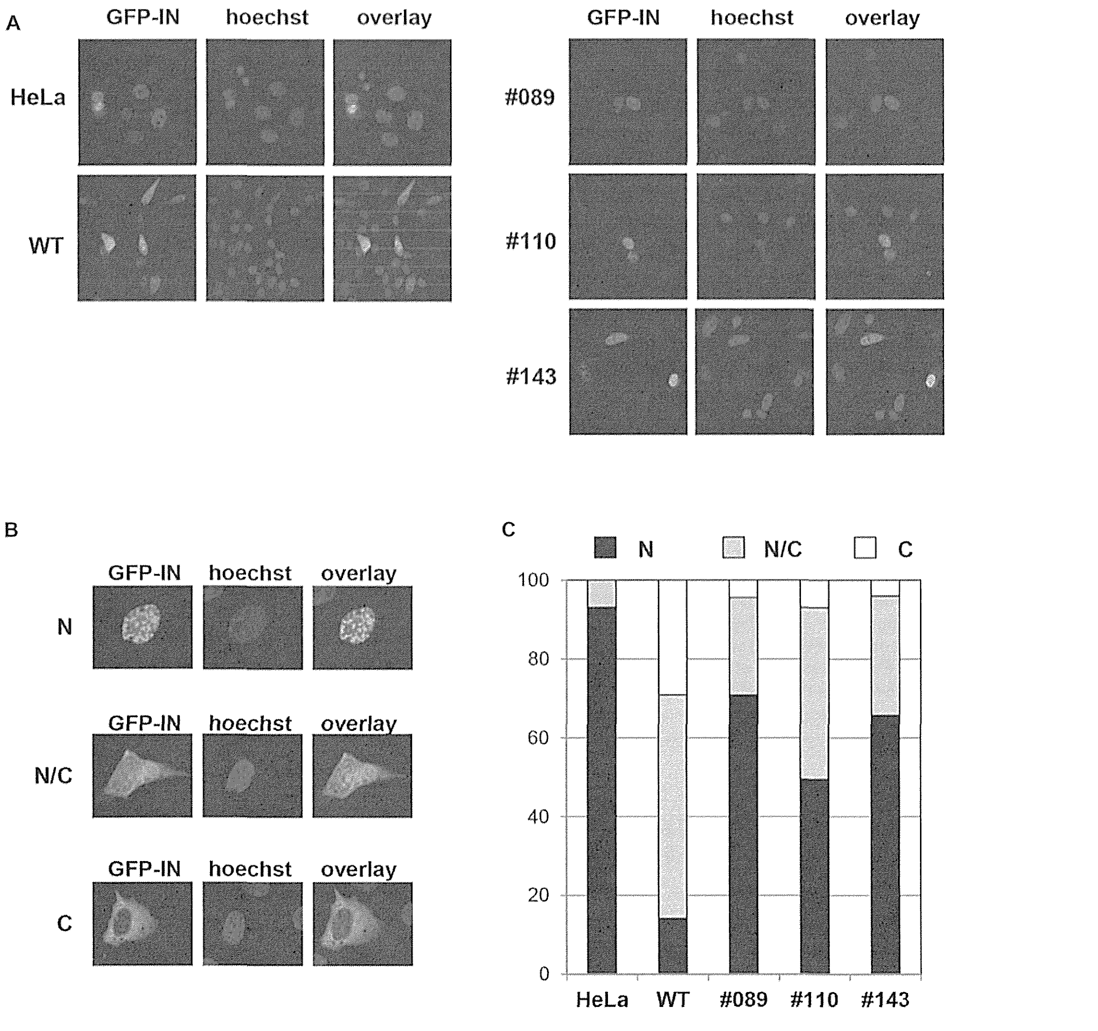

FIGURE 5 | Subcellular localization of GFP-IN in MEF cells. (A) HeLa and MEF cells were transfected with a plasmid expressing GFP-IN (green). After 48 h, cells were fixed and visualized by a confocal fluorescence microscopy. A typical distribution of GFP fluorescence is shown in MEF cells from different Tg lines. Hoechst (blue) was used to stain nuclear DNA. HeLa and WT MEF cells were used as a positive and negative control, respectively. **(B)** GFP positive cells were classified as follows; N, the fluorescence of GFP-IN is higher in the nucleus than in the cytoplasm; N/C, the fluorescence of GFP-IN in the nucleus is similar to the cytoplasm; and C, the fluorescence of GFP-IN is higher in the cytoplasm than in the nucleus. **(C)** GFP positive cells classified by (B) were quantified by counting approximately 100 cells.

mouse cells, probably by stably tethering the viral protein to chromatin as previously reported (Maertens et al., 2003; Llano et al., 2004b; Emiliani et al., 2005; Vanegas et al., 2005; Turlure et al., 2006).

THE SUSCEPTIBILITY OF hLEDGF/p75 Tg MEF CELLS TO HIV-1 INFECTION

Finally, we examined the susceptibility of MEF cells from hLEDGF/p75 Tg mice to HIV-1 infection. Tg (line No. 089, 110, and 143), WT, and LEDGF/p75 knockout MEF cells were infected with VSV-G-pseudotyped NL4-3 viruses, and then compared the efficiency of HIV-1 infection. We found that hLEDGF/p75 Tg MEF cells were significantly more susceptible to HIV-1 than WT and mLEDGF/p75 knockout MEF cells (**Figure 6**). It should be noted that the poor susceptibility of WT MEF cells to HIV-1 infection was almost equivalent to that of the mLEDGF/p75 knockout cells (**Figure 6**, left bar). Taken altogether, we conclude that hLEDGF/p75 is able to relieve the species barrier against HIV-1 infection in mouse cells by supporting HIV-1 PIC accumulation into the nucleus.

DISCUSSION

Pleiotropic functions of hLEDGF/p75 were suggested in HIV-1 infection including promotion of nuclear accumulation of PIC (Cherepanov et al., 2003, 2004; Maertens et al., 2003; Llano et al., 2004b; Ciuffi et al., 2005; Vanegas et al., 2005; Van Maele et al., 2006), selection of HIV-1 integration sites and enhancement of proviral integration (Bukrinsky, 2004; Llano et al., 2004a, 2006a; Emiliani et al., 2005). We previously showed that one of the species

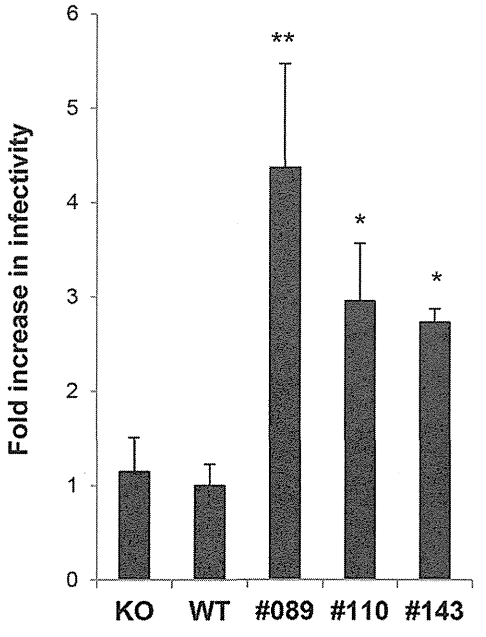

FIGURE 6 | Susceptibility of hLEDGF/p75 Tg MEF cells to HIV-1 infection. MEF cells derived from hLEDGF/p75 Tg, WT and LEDGF knockout (KO) mice were infected with an equivalent dose of VSV-G pseudotyped HIV-1 luciferase reporter virus. After 48 h, cells were lysed and subjected to luciferase assay. The data shown are the mean ± SD of triplicate experiments. $^{*}P < 0.05$, $^{**}P < 0.01$ (*t*-test).

barriers resides at the PIC nuclear accumulation step in mouse cells and that this restriction was caused by a dysfunction of the IN-dependent PIC accumulation system (Tsurutani et al., 2007).

In this study, we have generated 9 Tg mouse lines carrying hLEDGF/p75, to elucidate the role of LEDGF/p75 in the nuclear accumulation of IN. Among them, mice from line No. 089, 110, and 143 expressed hLEDGF/p75 in the thymus, spleen, lymph nodes and MEF cells. We found that the nuclear accumulation of HIV-1 IN in hLEDGF/p75 Tg MEF cells was greatly enhanced. Under these assay conditions, GFP-IN was less frequently localized to the nucleus in WT MEF cells. These results are consistent with the efficiency of luciferase expression after infection with HIV-1 pseudoviruses carrying a luciferase gene (**Figure 6**), suggesting that LEDGF/p75 is one of the host factors responsible for the HIV-1 species barrier.

The homology between hLEDGF/p75 and mLEDGF/p75 is high (92.3% amino acid identity). LEDGF/p75 is composed of four functional domains, the N-terminal Pro-Trp-Trp-Pro domain (residues 1–93), the C-terminal IN-binding domain (residues 347–429), the nuclear localization signal and the AT-hook DNA-binding motif (Maertens et al., 2003; Cherepanov et al., 2004, 2005; Vanegas et al., 2005; Llano et al., 2006a,b). The amino acid identity of these domains and motifs are completely matched between mouse and human LEDGF/p75. Therefore, it is likely that the species barrier in mouse cells might be caused by only small structural differences of previously underappreciated regions between mouse and human LEDGF/p75 proteins.

Shun et al. (2007) previously reported that HIV-1 integration was severely reduced in mLEDGF/p75 knockout mouse cells, suggesting that mLEDGF/p75 is able to support HIV-1 infection. In contrast, our data showed that the level of viral infectivity in WT MEF cells was almost equivalent to that in mLEDGF/p75 knockout cells used in the above report (Shun et al., 2007), rather suggesting that the mouse version might not contribute to the infection (**Figure 6**). This discrepancy might be due to the fact that our WT MEF cells are derived from the C3H/HeN mouse strain while mLEDGF/p75 knockout cells are derivatives of C57BL/6 mice. This needs to be elucidated with further experiments by comparison of different mouse strains. It should be noted that strain-specific epigenetic differences in mice, such as methylation patterns, have recently been reported (Schilling et al., 2009).

Small animal models for HIV-1 infection such as *Rag2*$^{-/-}$/*Il2rg*$^{-/-}$ mice (Traggiai et al., 2004) and BLT mice (Denton et al., 2008) have made significant contributions to our understanding of HIV/AIDS pathogenesis. However, the former mice show insufficient induction of an immune response against HIV-1 (Baenziger et al., 2006; An et al., 2007), while the use of latter mice has been influenced by some ethical restrictions and limited availability. On the other hand, immunologically intact transgenic mouse models are relatively straightforward and inexpensive, in which high levels of target gene expression can be easily achieved resulting in an obvious phenotype.

To generate humanized mouse models for HIV-1 infection, so far we have generated hCD4/hCXCR4/hCycT1 Tg mice and hCD4/hCCR5/hCycT1 Tg mice (Tsurutani et al., 2007). The addition of hLEDGF/p75 to these Tg mice should increase the susceptibility of these mice to HIV-1 infection, especially during the early phase of infection. However, we also need to pay attention to other host factors that restrict HIV-1 infection in mice, such as APOBEC3, which is an APOBEC-related cytidine deaminases (Kobayashi et al., 2004), because these inhibitors are also active in mouse cells (Yu et al., 2003; Kobayashi et al., 2004; Mous et al., 2012). Further characterization and identification of factors involved in host range barriers that are also present in the late phase of the viral replication cycle (transcription, RNA, export, and virion budding) should provide a new insight into the molecular mechanisms of HIV-1 replication and clues to the development of new therapeutics.

ACKNOWLEDGMENTS

We thank Ms. S. Kubo for her technical assistance and all of the members of our laboratory for their excellent animal care. We are grateful to A. Engelman (Harvard Medical School, Massachusetts, USA) for providing us with LEDGF knockout MEF cells. Kenzo Tokunaga is supported by grants from the Ministry of Health, Labor, and Welfare of Japan (Research on HIV/AIDS project no.H24-005, H24-008, and H25-010). Yoichiro Iwakura is supported by CREST program of the Japan Science and Technology Agency, the Promotion of Basic Research Activities for Innovative Biosciences, and Grants-in Aid from the Ministry of Education, Culture, Sports, Science, and Technology of Japan. The funders had no role in study design, data collection and analysis, decision to publish, or preparation of the manuscript.

AUTHOR CONTRIBUTIONS

Takuya Tada performed the experiments, analyzed the data and wrote the paper. Motohiko Kadoki analyzed the data. Yang Liu performed the experiments. Kenzo Tokunaga supervised the research, analyzed the data, and wrote the paper. Yoichiro Iwakura designed the study, supervised the work, analyzed data, and wrote the paper.

REFERENCES

An, D. S., Poon, B., Ho Tsong Fang, R., Weijer, K., Blom, B., Spits, H., et al. (2007). Use of a novel chimeric mouse model with a functionally active human immune system to study human immunodeficiency virus type 1 infection. *Clin. Vaccine Immunol.* 14, 391–396. doi: 10.1128/CVI.00403-406

Baenziger, S., Tussiwand, R., Schlaepfer, E., Mazzucchelli, L., Heikenwalder, M., Kurrer, M. O., et al. (2006). Disseminated and sustained HIV infection in CD34+ cord blood cell-transplanted Rag2-/- gamma c-/- mice. *Proc. Natl. Acad. Sci. U.S.A.* 103, 15951–15956. doi: 10.1073/pnas.0604493103

Berson, J. F., Long, D., Doranz, B. J., Rucker, J., Jirik, F. R., and Doms, R. W. (1996). A seven-transmembrane domain receptor involved in fusion and entry of T-cell-tropic human immunodeficiency virus type 1 strains. *J. Virol.* 70, 6288–6295.

Bieniasz, P. D., Grdina, T. A., Bogerd, H. P., and Cullen, B. R. (1998). Recruitment of a protein complex containing Tat and cyclin T1 to TAR governs the species specificity of HIV-1 Tat. *EMBO J.* 17, 7056–7065. doi: 10.1093/emboj/17.23.7056

Browning, J., Horner, J. W., Pettoello-Mantovani, M., Raker, C., Yurasov, S., Depinho, R. A., et al. (1997). Mice transgenic for human CD4 and CCR5 are susceptible to HIV infection. *Proc. Natl. Acad. Sci. U.S.A.* 94, 14637–14641. doi: 10.1073/pnas.94.26.14637

Bukrinsky, M. (2004). A hard way to the nucleus. *Mol. Med.* 10, 1–5.

Cherepanov, P., Devroe, E., Silver, P. A., and Engelman, A. (2004). Identification of an evolutionarily conserved domain in human lens epithelium-derived growth factor/transcriptional co-activator p75 (LEDGF/p75) that binds HIV-1 integrase. *J. Biol. Chem.* 279, 48883–48892. doi: 10.1074/jbc.M406307200

Cherepanov, P., Maertens, G., Proost, P., Devreese, B., Van Beeumen, J., Engelborghs, Y., et al. (2003). HIV-1 integrase forms stable tetramers and associates with LEDGF/p75 protein in human cells. *J. Biol. Chem.* 278, 372–381. doi: 10.1074/jbc.M209278200

Cherepanov, P., Sun, Z. Y., Rahman, S., Maertens, G., Wagner, G., and Engelman, A. (2005). Solution structure of the HIV-1 integrase-binding domain in LEDGF/p75. *Nat. Struct. Mol. Biol.* 12, 526–532. doi: 10.1038/nsmb937

Chomczynski, P., and Sacchi, N. (1987). Single-step method of RNA isolation by acid guanidinium thiocyanate-phenol-chloroform extraction. *Anal. Biochem.* 162, 156–159. doi: 10.1006/abio.1987.9999

Ciuffi, A., Llano, M., Poeschla, E., Hoffmann, C., Leipzig, J., Shinn, P., et al. (2005). A role for LEDGF/p75 in targeting HIV DNA integration. *Nat. Med.* 11, 1287–1289. doi: 10.1038/nm1329

Denton, P. W., Estes, J. D., Sun, Z., Othieno, F. A., Wei, B. L., Wege, A. K., et al. (2008). Antiretroviral pre-exposure prophylaxis prevents vaginal transmission of HIV-1 in humanized BLT mice. *PLoS Med.* 5:e16. doi: 10.1371/journal.pmed.0050016

Dragic, T., Charneau, P., Clavel, F., and Alizon, M. (1992). Complementation of murine cells for human immunodeficiency virus envelope/CD4-mediated fusion in human/murine heterokaryons. *J. Virol.* 66, 4794–4802.

Emiliani, S., Mousnier, A., Busschots, K., Maroun, M., Van Maele, B., Tempe, D., et al. (2005). Integrase mutants defective for interaction with LEDGF/p75 are impaired in chromosome tethering and HIV-1 replication. *J. Biol. Chem.* 280, 25517–25523. doi: 10.1074/jbc.M501378200

Feng, Y., Broder, C. C., Kennedy, P. E., and Berger, E. A. (1996). HIV-1 entry cofactor: functional cDNA cloning of a seven-transmembrane, G protein-coupled receptor. *Science* 272, 872–877. doi: 10.1126/science.272.5263.872

Fouchier, R. A., Meyer, B. E., Simon, J. H., Fischer, U., and Malim, M. H. (1997). HIV-1 infection of non-dividing cells: evidence that the amino-terminal basic region of the viral matrix protein is important for Gag processing but not for post-entry nuclear import. *EMBO J.* 16, 4531–4539. doi: 10.1093/emboj/16.15.4531

Ge, H., Si, Y., and Roeder, R. G. (1998a). Isolation of cDNAs encoding novel transcription coactivators p52 and p75 reveals an alternate regulatory mechanism of transcriptional activation. *EMBO J.* 17, 6723–6729. doi: 10.1093/emboj/17.22.6723

Ge, H., Si, Y., and Wolffe, A. P. (1998b). A novel transcriptional coactivator, p52, functionally interacts with the essential splicing factor ASF/SF2. *Mol. Cell* 2, 751–759. doi: 10.1016/S1097-2765(00)80290-7

Iwabu, Y., Fujita, H., Kinomoto, M., Kaneko, K., Ishizaka, Y., Tanaka, Y., et al. (2009). HIV-1 accessory protein Vpu internalizes cell-surface BST-2/tetherin through transmembrane interactions leading to lysosomes. *J. Biol. Chem.* 284, 35060–35072. doi: 10.1074/jbc.M109.058305

Iwakura, Y., Shioda, T., Tosu, M., Yoshida, E., Hayashi, M., Nagata, T., et al. (1992). The induction of cataracts by HIV-1 in transgenic mice. *AIDS* 6, 1069–1075. doi: 10.1097/00002030-199210000-00002

Kobayashi, M., Takaori-Kondo, A., Shindo, K., Abudu, A., Fukunaga, K., and Uchiyama, T. (2004). APOBEC3G targets specific virus species. *J. Virol.* 78, 8238–8244. doi: 10.1128/JVI.78.15.8238-8244.2004

Llano, M., Delgado, S., Vanegas, M., and Poeschla, E. M. (2004a). Lens epithelium-derived growth factor/p75 prevents proteasomal degradation of HIV-1 integrase. *J. Biol. Chem.* 279, 55570–55577. doi: 10.1074/jbc.M408508200

Llano, M., Vanegas, M., Fregoso, O., Saenz, D., Chung, S., Peretz, M., et al. (2004b). LEDGF/p75 determines cellular trafficking of diverse lentiviral but not murine oncoretroviral integrase proteins and is a component of functional lentiviral preintegration complexes. *J. Virol.* 78, 9524–9537. doi: 10.1128/JVI.78.17.9524-9537.2004

Llano, M., Saenz, D. T., Meehan, A., Wongthida, P., Peretz, M., Walker, W. H., et al. (2006a). An essential role for LEDGF/p75 in HIV integration. *Science* 314, 461–464. doi: 10.1126/science.1132319

Llano, M., Vanegas, M., Hutchins, N., Thompson, D., Delgado, S., and Poeschla, E. M. (2006b). Identification and characterization of the chromatin-binding domains of the HIV-1 integrase interactor LEDGF/p75. *J. Mol. Biol.* 360, 760–773. doi: 10.1016/j.jmb.2006.04.073

Lores, P., Boucher, V., Mackay, C., Pla, M., Von Boehmer, H., Jami, J., et al. (1992). Expression of human CD4 in transgenic mice does not confer sensitivity to human immunodeficiency virus infection. *AIDS Res. Hum. Retroviruses* 8, 2063–2071. doi: 10.1089/aid.1992.8.2063

Maddon, P. J., Littman, D. R., Godfrey, M., Maddon, D. E., Chess, L., and Axel, R. (1985). The isolation and nucleotide sequence of a cDNA encoding the T cell surface protein T4: a new member of the immunoglobulin gene family. *Cell* 42, 93–104. doi: 10.1016/S0092-8674(85)80105-7

Maertens, G., Cherepanov, P., Pluymers, W., Busschots, K., De Clercq, E., Debyser, Z., et al. (2003). LEDGF/p75 is essential for nuclear and chromosomal targeting of HIV-1 integrase in human cells. *J. Biol. Chem.* 278, 33528–33539. doi: 10.1074/jbc.M303594200

Maillot, B., Levy, N., Eiler, S., Crucifix, C., Granger, F., Richert, L., et al. (2013). Structural and functional role of INI1 and LEDGF in the HIV-1 preintegration complex. *PLoS ONE* 8:e60734. doi: 10.1371/journal.pone.0060734

Mariani, R., Rasala, B. A., Rutter, G., Wiegers, K., Brandt, S. M., Krausslich, H. G., et al. (2001). Mouse-human heterokaryons support efficient human immunodeficiency virus type 1 assembly. *J. Virol.* 75, 3141–3151. doi: 10.1128/JVI.75.7.3141-3151.2001

Mariani, R., Rutter, G., Harris, M. E., Hope, T. J., Krausslich, H. G., and Landau, N. R. (2000). A block to human immunodeficiency virus type 1 assembly in murine cells. *J. Virol.* 74, 3859–3870. doi: 10.1128/JVI.74.8.3859-3870.2000

Mous, K., Jennes, W., Camara, M., Seydi, M., Daneau, G., Mboup, S., et al. (2012). Expression analysis of LEDGF/p75, APOBEC3G, TRIM5alpha, and tetherin in a Senegalese cohort of HIV-1-exposed seronegative individuals. *PLoS ONE* 7:e33934. doi: 10.1371/journal.pone.0033934

Niwa, H., Yamamura, K., and Miyazaki, J. (1991). Efficient selection for high-expression transfectants with a novel eukaryotic vector. *Gene* 108, 193–199. doi: 10.1016/0378-1119(91)90434-D

Saijo, S., Fujikado, N., Furuta, T., Chung, S. H., Kotaki, H., Seki, K., et al. (2007). Dectin-1 is required for host defense against Pneumocystis carinii but not against Candida albicans. *Nat. Immunol.* 8, 39–46. doi: 10.1038/ni1425

Sawada, S., Gowrishankar, K., Kitamura, R., Suzuki, M., Suzuki, G., Tahara, S., et al. (1998). Disturbed CD4+ T cell homeostasis and in vitro HIV-1 susceptibility in transgenic mice expressing T cell line-tropic HIV-1 receptors. *J. Exp. Med.* 187, 1439–1449. doi: 10.1084/jem.187.9.1439

Schilling, E., El Chartouni, C., and Rehli, M. (2009). Allele-specific DNA methylation in mouse strains is mainly determined by cis-acting sequences. *Genome Res.* 19, 2028–2035. doi: 10.1101/gr.095562.109

Shun, M. C., Raghavendra, N. K., Vandegraaff, N., Daigle, J. E., Hughes, S., Kellam, P., et al. (2007). LEDGF/p75 functions downstream from preintegration complex formation to effect gene-specific HIV-1 integration. *Genes Dev.* 21, 1767–1778. doi: 10.1101/gad.1565107

Singh, D. P., Ohguro, N., Chylack, L. T. Jr., and Shinohara, T. (1999). Lens epithelium-derived growth factor: increased resistance to thermal and oxidative stresses. *Invest. Ophthalmol. Vis. Sci.* 40, 1444–1451.

Smith, D. R., and Murphy, D. (1993). Genomic analysis of transgenic animals: southern blotting. *Methods Mol. Biol.* 18, 323–327. doi: 10.1385/0-89603-245-0:323

Tokunaga, K., Greenberg, M. L., Morse, M. A., Cumming, R. I., Lyerly, H. K., and Cullen, B. R. (2001). Molecular basis for cell tropism of CXCR4-dependent human immunodeficiency virus type 1 isolates. *J. Virol.* 75, 6776–6785. doi: 10.1128/JVI.75.15.6776-6785.2001

Tokunaga, K., Kojima, A., Kurata, T., Ikuta, K., Akari, H., Koyama, A. H., et al. (1998). Enhancement of human immunodeficiency virus type 1 infectivity by Nef is producer cell-dependent. *J. Gen. Virol.* 79(Pt 10), 2447–2453.

Traggiai, E., Chicha, L., Mazzucchelli, L., Bronz, L., Piffaretti, J. C., Lanzavecchia, A., et al. (2004). Development of a human adaptive immune system in cord blood cell-transplanted mice. *Science* 304, 104–107. doi: 10.1126/science.1093933

Tsurutani, N., Yasuda, J., Yamamoto, N., Choi, B. I., Kadoki, M., and Iwakura, Y. (2007). Nuclear import of the preintegration complex is blocked upon infection by human immunodeficiency virus type 1 in mouse cells. *J. Virol.* 81, 677–688. doi: 10.1128/JVI.00870-876

Turlure, F., Maertens, G., Rahman, S., Cherepanov, P., and Engelman, A. (2006). A tripartite DNA-binding element, comprised of the nuclear localization signal and two AT-hook motifs, mediates the association of LEDGF/p75 with chromatin in vivo. *Nucleic Acids Res.* 34, 1653–1665. doi: 10.1093/nar/gkl052

van Maanen, M., and Sutton, R. E. (2003). Rodent models for HIV-1 infection and disease. *Curr. HIV Res.* 1, 121–130. doi: 10.2174/1570162033352075

Van Maele, B., Busschots, K., Vandekerckhove, L., Christ, F., and Debyser, Z. (2006). Cellular co-factors of HIV-1 integration. *Trends Biochem. Sci.* 31, 98–105. doi: 10.1016/j.tibs.2005.12.002

Vanegas, M., Llano, M., Delgado, S., Thompson, D., Peretz, M., and Poeschla, E. (2005). Identification of the LEDGF/p75 HIV-1 integrase-interaction domain and NLS reveals NLS-independent chromatin tethering. *J. Cell Sci.* 118, 1733–1743. doi: 10.1242/jcs.02299

Wei, P., Garber, M. E., Fang, S. M., Fischer, W. H., and Jones, K. A. (1998). A novel CDK9-associated C-type cyclin interacts directly with HIV-1 Tat and mediates its high-affinity, loop-specific binding to TAR RNA. *Cell* 92, 451–462. doi: 10.1016/S0092-8674(00)80939-3

Yasuda, J., Miyao, T., Kamata, M., Aida, Y., and Iwakura, Y. (2001). T cell apoptosis causes peripheral T cell depletion in mice transgenic for the HIV-1 vpr gene. *Virology* 285, 181–192. doi: 10.1006/viro.2001.0964

Yu, X., Yu, Y., Liu, B., Luo, K., Kong, W., Mao, P., et al. (2003). Induction of APOBEC3G ubiquitination and degradation by an HIV-1 Vif-Cul5-SCF complex. *Science* 302, 1056–1060. doi: 10.1126/science.1089591

Conflict of Interest Statement: The authors declare that the research was conducted in the absence of any commercial or financial relationships that could be construed as a potential conflict of interest.

Received: 11 October 2013; accepted: 22 November 2013; published online: 17 December 2013.

Citation: Tada T, Kadoki M, Liu Y, Tokunaga K and Iwakura Y (2013) Transgenic expression of the human LEDGF/p75 gene relieves the species barrier against HIV-1 infection in mouse cells. Front. Microbiol. 4:377. doi: 10.3389/fmicb.2013.00377

This article was submitted to Virology, a section of the journal Frontiers in Microbiology.

APOBEC3G Oligomerization Is Associated with the Inhibition of Both *Alu* and LINE-1 Retrotransposition

Takayoshi Koyama[1©], Juan Fernando Arias[1©], Yukie Iwabu[1], Masaru Yokoyama[2], Hideaki Fujita[3], Hironori Sato[2], Kenzo Tokunaga[1*]

1 Department of Pathology, National Institute of Infectious Diseases, Tokyo, Japan, 2 Pathogen Genomics Center, National Institute of Infectious Diseases, Tokyo, Japan, 3 Faculty of Pharmaceutical Sciences, Nagasaki International University, Nagasaki, Japan

Abstract

Alu and LINE-1 (L1), which constitute ~11% and ~17% of the human genome, respectively, are transposable non-LTR retroelements. They transpose not only in germ cells but also in somatic cells, occasionally causing cancer. We have previously demonstrated that antiretroviral restriction factors, human APOBEC3 (hA3) proteins (A–H), differentially inhibit L1 retrotransposition. In this present study, we found that hA3 members also restrict *Alu* retrotransposition at differential levels that correlate with those observed previously for L1 inhibition. Through deletion analyses based on the best-characterized hA3 member human APOBEC3G (hA3G), its N-terminal 30 amino acids were required for its inhibitory activity against *Alu* retrotransposition. The inhibitory effect of hA3G on *Alu* retrotransposition was associated with its oligomerization that was affected by the deletion of its N-terminal 30 amino acids. Through structural modeling, the amino acids 24 to 28 of hA3G were predicted to be located at the interface of the dimer. The mutation of these residues resulted in abrogated hA3G oligomerization, and consistently abolished the inhibitory activity of hA3G against *Alu* retrotransposition. Importantly, the anti-L1 activity of hA3G was also associated with hA3G oligomerization. These results suggest that the inhibitory activities of hA3G against *Alu* and L1 retrotransposition might involve a common mechanism.

Citation: Koyama T, Arias JF, Iwabu Y, Yokoyama M, Fujita H, et al. (2013) APOBEC3G Oligomerization Is Associated with the Inhibition of Both *Alu* and LINE-1 Retrotransposition. PLoS ONE 8(12): e84228. doi:10.1371/journal.pone.0084228

Editor: Chen Liang, Lady Davis Institute for Medical Research, Canada

Received October 23, 2013; **Accepted** November 20, 2013; **Published** December 19, 2013

Funding: This work was supported by grants from the Ministry of Health, Labor and Welfare of Japan (Research on HIV/AIDS project no.H24-005, H24-008 and H25-010), and from the Ministry of Education, Science, Technology, Sports and Culture of Japan (22590428). The funders had no role in study design, data collection and analysis, decision to publish, or preparation of the manuscript.

Competing interests: The authors have declared that no competing interests exist.

* Email: tokunaga@nih.go.jp

© These authors contributed equally to this work.

Introduction

Retrotransposons compose ~42% of the human genome, and these elements are classified into the non-LTR and LTR classes. Non-LTR retrotransposons are subdivided into long interspersed elements (LINEs) and short interspersed elements (SINEs), representatives of which are LINE-1 (L1) and *Alu*, which comprise ~17% and ~11% of the human genome, respectively [1]. L1 elements harbor two ORFs: ORF1, which encodes an RNA-binding protein, and ORF2, which encodes an endonuclease-like and reverse transcriptase-like protein. After translation, these proteins bind to the L1 RNA to form a ribonucleoprotein particle that is imported into the nucleus to be integrated into the genome through target-primed reverse transcription [2-4]. Unlike L1, *Alu* elements do not encode a reverse transcriptase or an endonuclease; rather, the transcribed *Alu* RNAs hijack the L1-encoded enzymes to move to new locations in the genome through mechanisms that are as yet unclear [5]. Importantly, retrotransposition by L1 and *Alu* occurs not only in germ cells, causing several genetic diseases [6-13], but also in somatic cells, such as brain tissues [14,15], and malignant tissues and cells such as B-cell lymphoma cells [16], breast carcinoma tissue [17], colon carcinoma tissue [18], and hepatocellular carcinoma tissue [19]. These facts indicate that an intrinsic protection system should function properly to suppress these types of retrotransposition in normal somatic cells.

Human APOBEC3G (hA3G) is one of the seven members of the APOBEC3 (hA3) family of cytidine deaminases (hA3A to hA3H). hA3G is known to be an intrinsic retroviral restriction factor that inhibits Vif-defective human immunodeficiency virus type 1 (HIV-1) infection by being incorporated into viral particles and mediating extensive deamination of the nascent minus-strand viral DNA during reverse transcription, which results in G-to-A hypermutation [20-23]. This antiretroviral restriction extends to not only exogenous retroviruses, such as simian immunodeficiency virus [24-27], primate foamy virus [28,29], human T-cell leukemia virus type I [30], murine leukemia virus [21,26,31], mouse mammary tumor virus [32], and equine infectious anemia virus [22] , but also endogenous retroelements, such as the MusD and intracisternal A-particle LTR murine retrotransposons and, as described below, human *Alu* and L1 retrotransposons ([33-40]; see also review in ref[41].). hA3G also restricts infection by hepatitis B virus, which replicates its DNA genome by reverse transcription of an RNA intermediate [42,43]. Whereas pre-primate mammals encode one, two to three A3 proteins [44], primates have acquired seven different A3 genes through 33 million years of evolution [45]. Such expansion of the hA3 genes correlates with an abrupt reduction in retrotransposition activity in primates, suggesting that these proteins have evolved to protect hosts from the genomic instability caused by retroelements [46].

We previously reported that hA3 family proteins have differential levels of anti-L1 activity that do not correlate with either antiretroviral activity or subcellular localization patterns [37]. Although several groups that performed similar studies showed that hA3G has little or no anti-L1 activity [47-50], we and others have found that the hA3G is indeed able, albeit less potently than hA3A or hA3B, to restrict L1 retrotransposition [37-40]. Such discrepancies might be attributed to the cell-type-dependent expression levels of hA3G, as we previously demonstrated [37]. We also found that hA3G inhibits L1 retrotransposition independently of its deaminase activity, which is primarily required for its antiretroviral function, and hA3G likely prevents L1 DNA synthesis *per se* [37]. With regard to the inhibition of *Alu* by hA3 family members, several groups have reported that hA3A, hA3B [49], hA3G [34-36], hA3DE, and hA3H [51] inhibit *Alu* retrotransposition. In this study, we found that all hA3 family members, from hA3A to hA3H, are able to inhibit *Alu* retrotransposition. The inhibitory effect of hA3G on *Alu* retrotransposon was associated with the N-terminal 30 amino acid residues and with hA3G's oligomerization activity, but not with its deaminase activity. Structural modeling showed that amino acid positions 24–28 are responsible for the oligomerization of hA3G. This result was verified by immunoprecipitation using an hA3G mutant with amino acid substitutions at these positions. Consistent with this result, we found that amino acid positions 24–28 of hA3G are critical for its inhibitory activity against *Alu* retrotransposon. Importantly, these amino acids were also shown to be important for L1 inhibition, suggesting that both *Alu* and L1 retrotransposition might be restricted by similar mechanisms involving hA3G, which require the oligomerization of this restriction factor.

Materials and Methods

DNA constructs

The hemagglutinin (HA)-tagged hA3 expression plasmids (phA3A-HA, phA3B-HA, phA3C-HA, phA3DE-HA, phA3F-HA, phA3G-HA, and phA3H-HA), the GFP expression plasmid pCA-EGFP, the empty expression vector pCAGGS-HA, the L1 indicator construct pCEP4/L1mneoI/ColE1 (kindly provided by N. Gilbert), the L1 ORF2 expression plasmid pBudORF2opt (kindly provided by A.M. Roy-Engel), the *Alu* indicator construct pYa5neotet (kindly provided by T. Heidmann), Vif-deficient HIV-1 proviral indicator construct pNLLuc-F(-)E(-), and VSV-G expression plasmid pHIT/G have previously been described elsewhere [5,37,52-55] (note that the hA3h expression plasmid encodes the haplotype I). The myc-tagged version of the wild-type hA3G expression plasmid, phA3G-myc, was also created. A series of N-terminal deletion mutants of hA3G (phA3G-NΔ30-HA, -NΔ60-HA, -NΔ90-HA, -NΔ120-HA, and -NΔ150-HA) were created by inserting serially deleted PCR fragments of hA3G into the mammalian expression plasmid pCAGGS with a C-terminal HA-tag. The deaminase-deficient mutant (phA3G-E259Q-HA), the oligomerization-deficient mutant (phA3G-C97/100A-HA), and the N-terminal mutants (phA3G-5G(24–28)-HA, phA3G-4G(124–127)-HA, phA3G-R24G-HA, and phA3G-Y125G-HA) of hA3G were created using phA3G-HA as a template with a QuikChange site-directed mutagenesis kit (Stratagene).

Cell maintenance, transfections, and protein analyses

HeLa and 293T cells were maintained under standard conditions. 293T cells were transfected with HA-tagged hA3 wild-type and mutant plasmids using the FuGENE 6 transfection reagent (Roche Applied Science) according to the manufacturer's instructions. Cell extracts from transfected cells were subjected to gel electrophoresis and then transferred to a nitrocellulose membrane. The membranes were probed with an anti-HA mouse monoclonal antibody (Sigma). The antibody-bound proteins were visualized to confirm hA3 protein expression by chemiluminescence using an ECL Western blotting detection system (GE Healthcare) and an LAS-3000 imaging system (FujiFilm).

Immunofluorescence microscopy

HeLa cells were plated on 13-mm glass coverslips and transfected with 0.5 µg of hA3 expressing plasmids by using FUGENE6. The transfected cells were fixed with 4% paraformaldehyde at room temperature for 30 min, permeabilized with 0.05% saponin for 10 min, and immunostained with an anti-HA monoclonal antibody (5 µg/ml). The secondary goat anti-mouse antibody that was conjugated with Cy3 was used at 5 µg/ml. All immunofluorescence images were observed on a Leica DMRB microscope (Wetzlar, Germany) equipped with a 63×1.32 NA oil immersion lens (PL APO), acquired through a cooled CCD camera, MicroMAX (Princeton Instruments, Trenton, NJ), and digitally processed using IPlab Software (Scanalytics, Fairfax, VA). All images were assembled using Adobe Photoshop (Adobe Systems, Mountain View, CA).

L1 and Alu retrotransposition assay

L1 and *Alu* retrotransposition assays were performed by co-transfecting 2 x 10^5 HeLa cells with 0.1 µg of the respective hA3 expression plasmid (or a mock expression vector, pCAGGS-HA, as a positive control) together with either 0.3 µg of the neomycin-resistance (neo^r)-based L1 expression vector pCEP4/L1mneoI/ColE1 and 0.1 µg of an empty vector (for the

L1 retrotransposition assay) or 0.3 µg of the neo^r-based *Alu* expression vector pYa5neotet and 0.1 µg of the L1 ORF2 expression plasmid pBudORF2opt (for the *Alu* retrotransposition assay) using Lipofectamine and Plus reagents (Invitrogen). As a negative control, 0.5 µg of a GFP expression vector, pCA-EGFP, was transfected into HeLa cells. After 72 h, the cells were trypsinized, re-seeded into T25 or T75 flasks for G418 selection (1 mg/ml for the L1 assay and 400 µg/ml for the *Alu* assay), and maintained. At 14 days after selection, the resultant G418-resistant (G418^R) colonies were fixed, stained with crystal violet (Merck), and counted.

Oligomerization assay

To perform a coimmunoprecipitation-based oligomerization assay, plasmids (0.5 µg) expressing HA-tagged wild-type and mutant hA3G were transfected along with phA3G-myc (0.5 µg) into 293T cells using FuGENE 6. After 48 h, the transfected cells were suspended in 500 µl of RIPA buffer (50 mM Tris-HCl, pH 7.4, 150 mM NaCl, 1% NP-40, 0.5% sodium deoxycholate, 0.1% SDS, complete protease inhibitor cocktail [Roche]). The resultant lysates were clarified by brief centrifugation, pre-cleared with 30 µl of Protein A-Agarose Fast Flow (GE Healthcare) for 1 h at 4°C, and then incubated with an anti-myc affinity gel (Sigma). After 1 h at 4°C, the immune complexes were extensively washed with RIPA buffer. Equal aliquots of the total and bound fractions were subjected to gel electrophoresis and transferred to a nitrocellulose membrane. The membranes were probed with an anti-HA mouse monoclonal antibody (Sigma) or an anti-β-actin mouse monoclonal antibody (AC-74, Sigma). The signal intensities of the immunoprecipitated hA3G protein on Western blots were quantified using the LAS-3000 imaging system (Fujifilm). For the RNase A treatment experiment, the immune complexes were separated into two aliquots. The wild-type sample was incubated with or without 25 U of RNase A (Sigma) at room temperature for 30 min. Samples were extensively washed and then resuspended in loading dye. The samples were assayed as described above.

Molecular modeling of the head-to-head dimer structure of the N-terminus of hA3G

Head-to-head dimer models of hA3G N-terminal domain were obtained by homology modelling using either the crystal structure of human APOBEC2 (hA2) at a resolution of 2.50 Å or the NMR structure of the C-terminal domain of hA3G (PDB code: 2NYT chain A [56] or 2JYW [57], respectively) as a template, as previously performed [34,58-60]. To minimize misalignments between the hA3G N-terminal domain as a target sequence and either hA2 or the C-terminal domain of hA3G as a template sequence, we used the multiple sequence alignment method with the sequences of hA3A (GenBank accession number: NM_145699), hA3C (GenBank accession number: NM_014508), and hA3F (GenBank accession number: NM_145298). Multiple sequence alignments were generated using 'MOE-Align' in Molecular Operating Environment (MOE) version 2010.10 (Chemical Computing Group Inc., Quebec, Canada). Three-dimensional (3-D) models of the hA3G N-terminal domain were constructed by the homology modeling technique using 'MOE-Homology' in MOE as previously described [61]. We obtained 25 intermediate models per homology modeling session in MOE, and we selected the 3-D models that were intermediate models with best scores according to the generalized Born/volume integral methodology [62]. The 3-D structure was thermodynamically optimized by energy minimization using MOE and an AMBER99 force field [63] combined with the generalized Born model of aqueous solvation implemented in MOE [64]. The physically unacceptable local structure of the optimized 3-D model was further refined based on the evaluation of the Ramachandran plot using MOE.

Results

hA3 family members differentially inhibit Alu retrotransposition

To determine if hA3 family members are able to inhibit *Alu* retrotransposition as well as L1 retrotransposition [37], we performed a neo^r-based retrotransposition assay [5]. In this assay system, we utilized a L1 ORF2 expression plasmid that is required for *Alu* retrotransposition [53], together with an *Alu* clone DNA carrying a reverse-oriented neo^r gene separated by a gamma-globin intron. After transfection of the cells with this construct, neo^r with *Alu* is transcribed, spliced, reverse-transcribed, and integrated. Then, the neo^r gene that is integrated with *Alu* is driven by the CMV promoter and expressed. After G418 selection following transfection, we were able to quantify the retrotransposition level by counting the number of G418^R colonies. hA3 protein expression in the cells were confirmed by immunoblotting using anti-HA antibodies (Figure 1A). Without the co-expression of an hA3 protein, *Alu* retrotransposition occurred at the level shown in the upper left panel of Figure 1B. In contrast, the co-expression of any of the hA3 proteins differentially inhibited *Alu* retrotransposition, and in particular, the expression of hA3A, hA3B, or hA3G strongly decreased the transposition level of *Alu* elements (Figure 1C). Thus, we conclude that hA3 proteins act to differentially suppress *Alu* retrotransposition. Importantly, in agreement with previous reports [34-36,39], we observed that hA3G has an inhibitory effect on *Alu* retrotransposition in the assay. It should be noted that these activities against *Alu* correlated exactly with the patterns previously observed for the inhibition of L1 [37].

The *N*-terminal 30 amino acids of hA3G determine the inhibitory effect on Alu retrotransposition

Because hA3G is the best characterized hA3 family member protein, we focused on this protein and attempted to determine the region responsible for its anti-retrotransposon activities. To identify the relevant region, we created a series of mutants with serial deletions from the N-terminus up to amino residue 150 (Figure 2A). Protein expression in the cells transfected with each plasmid was confirmed by immunoblotting using an anti-HA antibody (Figure 2B). hA3G mutants lacking the C-terminal domain were undetectable as previously reported [34,65] and therefore could not be used for further experiments. Immunofluorescence microscopy confirmed that hA3G deletion

Figure 1

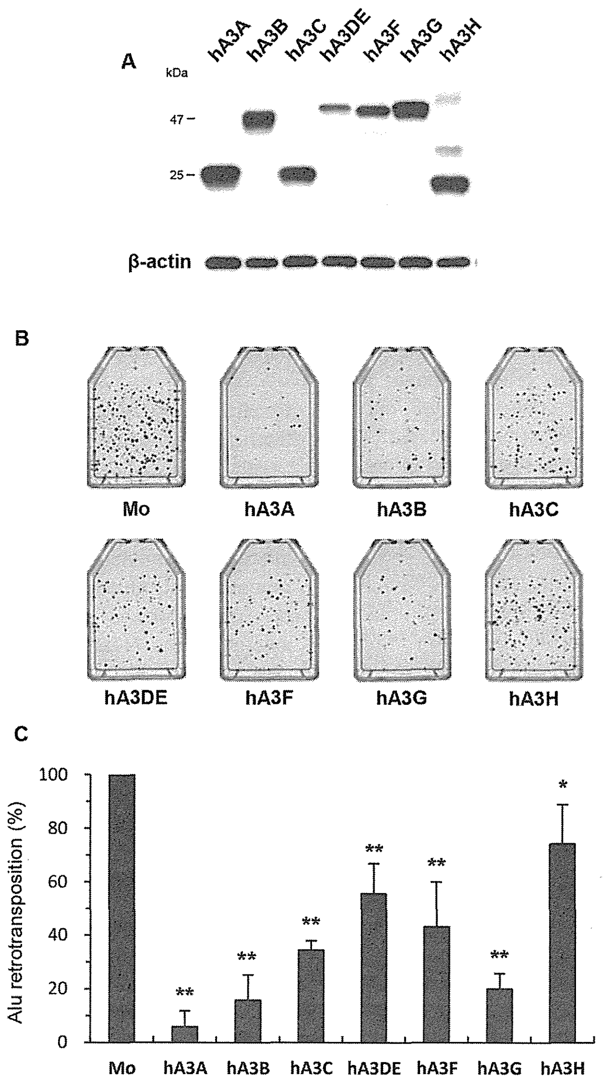

Figure 1. hA3 proteins inhibit Alu retrotransposition at differential levels. (**A**) Western blot analysis was performed by using extracts from 293T cells transfected with HA-tagged hA3 expression plasmids. Antibodies specific for HA were used. (**B**, **C**) HeLa cells were cotransfected with the *neo*^{r}-based *Alu* expression vector pYa5neotet and the L1 ORF2 expression plasmid pBudORF2opt, together with the respective hA3 expression plasmid. Seventy-two hours later, the cells were trypsinized, re-seeded into T25 or T75 flasks, and subjected to G418 (400 µg/ml) selection. At 14 days after selection, the resultant G418^R colonies fixed, stained with crystal violet (B), and counted to determine the level of *Alu* retrotransposition (C). The retrotransposition level in the absence of hA3 proteins was set to 100%. The data shown are the mean ± SD of triplicate experiments. Mo, mock. $^*P < 0.05$, $^{**}P < 0.005$, *t*-test.

doi: 10.1371/journal.pone.0084228.g001

mutant proteins other than NΔ150 were predominantly localized to the cytoplasm, as was the wild-type protein (Figure 2C). These deletions also abrogated the anti-HIV-1 activity of hA3G (Figure S1). We performed an *Alu* retrotransposition assay by transfecting HeLa cells with the *Alu* expression plasmid, the L1 expression plasmid, and a wild-type or mutant hA3G plasmid, and we observed that the deletion of 30 or more residues from the N-terminus of hA3G completely abrogated the inhibitory activity of hA3G on *Alu* retrotransposition (Figures 2D and 2E). We therefore conclude that the N-terminal 30 amino acids of hA3G are critical for the inhibition of *Alu* retrotransposition.

The inhibitory effect of hA3G on Alu retrotransposition is associated with its oligomerization and is independent of its deaminase activity

The anti-HIV-1 activity of hA3G is known to be dependent on two different activities, deamination and oligomerization, the former of which has been shown to be disrupted by the mutation of E259 located in the C-terminal cytidine deaminase (CD2) [65,66], and the latter of which has been reported to be abrogated by the mutation of C97 and C100 located in the N-terminal cytidine deaminase (CD1) [65]. Based on these past findings, we wished to determine which functions of hA3G are crucial for blocking the ability of *Alu* to retrotranspose. We created plasmids expressing hA3G defective in either oligomerization or deamination (C97/100A or E259Q, respectively; Figure 3A) and confirmed the expression of these proteins by immunoblotting using an anti-HA antibody (Figure 3B). Interestingly, the *Alu* retrotransposition assay revealed that the C97/100A oligomerization mutant of hA3G had no inhibitory activity against *Alu* retrotransposition, whereas the E259Q deamination mutant retained wild-type activity (Figure 3C). These observations confirmed the previous results [34,35], showing that the inhibition of *Alu* retrotransposition by hA3G is not due to the ability of hA3G to deaminate this retrotransposon but is due to its ability to form an oligomer.

The *N*-terminal 30 amino acids of hA3G are required for the oligomerization of this protein

Because hA3G's inhibitory activity against *Alu* retrotransposition was abolished in the mutants carrying an N-terminal deletion of 30 or more residues (Figure 2) and in the oligomerization mutant harboring mutations at amino acid positions 97 and 100 (Figure 3), we reasoned that the N-terminal 30 amino acids of hA3G might be critical for its ability to form oligomers. To test this hypothesis, we performed an oligomerization assay by coexpressing wild-type hA3G tagged with Myc and the mutant hA3Gs tagged with HA. The cell lysates were then immunoprecipitated with an anti-HA antibody and immunoblotted with an anti-Myc antibody. As shown in Figure 4, the E259Q deamination mutant of myc-tagged hA3G was efficiently coimmunoprecipitated with the HA-tagged wild-type protein. In contrast, the N-terminal serial deletion mutants lacking 30 or more residues completely lost the ability to oligomerize, as did the C97/100A mutant. When the immunoprecipitated samples were treated with RNase A, the oligomerization efficiency of hA3G was moderately decreased (Figure S2), consistent with the previous reports that cellular RNA might contribute to the stabilization of hA3G's oligomer [34]. Thus, the 30 amino acids at the N-terminus of hA3G are responsible for its oligomerization.

The *N*-terminal 30 amino acids of hA3G are the structural key for its oligomerization

To fully understand the mechanism by which N-terminal 30 amino acids of hA3G regulate oligomerization, we analyzed the effect of the deletion of the N-terminal 30 amino acids on the predicted 3-D structure of the hA3G dimer that was reported to be the major form of hA3G oligomer [34,59]. Thermodynamically stable N-terminal structures of wild-type hA3G and its N-terminal 30-amino-acid deletion mutant were constructed by homology modeling using the hA2 crystal structure as a template. As shown in Figures 5A and B, when the structures of the wild-type and deletion mutant hA3G proteins were compared, it was obvious that the N-terminal 30 amino acids (shown in cyan in Figure 5A) were present along the contact surface of the hA3G dimer, and therefore, the deletion of this region could abolish the interaction interface between the two hA3G molecules. We thus conclude that the N-terminal 30 amino acid residues of hA3G are located at the dimer interface and are critical for oligomerization.

Residues 24–28 contribute to the ability of hA3G to homooligomerize and inhibit Alu retrotransposition

Next, we analyzed the interaction interface of the hA3G dimer by structural modeling based not only on the hA2 crystal structure but also on the C-terminal hA3G (hA3G-C) NMR structure in parallel. Both structural modeling of wild-type hA3G revealed that, among the N-terminal 30 amino acids, a cluster of dimer interface residues (R24, P25, I26, L27, and S28) located in the N-terminal core structure α1-loop-β1 of hA3G interact with the counterpart residues of another monomer (Figures 6A and 6B). Importantly, this interface corresponds structurally (but not genetically) to a part of the potential oligomerization interfaces of the hA3G C-terminal domain, as described by Shandilya et al. [67]. At this putative interaction surface (Figures 6A and 6B), R24 likely interacts with D130 of another monomer through hydrogen bonds and electrostatic interactions, whereas the isoleucine/leucine residues at positions 26/27 can form a hydrophobic interaction with the counterpart residues of another monomer. hA2-based modeling shows that the serine residue at position 28 forms another hydrogen bond with the counterpart residues of another monomer (Figure 6A), although the same residue in hA3G-C-based modeling appears to be slightly separated from the counterpart residue of another monomer (Figure 6B). Additionally, the structural stability would be enhanced by a proline residue at position 25 in the loop. Thus, we speculated that the mutation of these residues might abolish the oligomerization of hA3G. To test this hypothesis, we first addressed whether structural modeling would be able to distinguish oligomerization-deficient and oligomerization-intact hA3Gs by analyzing the model of an hA3G mutant (hA3G-4G(124–127)), in which we introduced the small amino acid glycine in place of the aromatic amino acid residues

Oligomerized hA3G inhibits retrotransposition

Figure 2

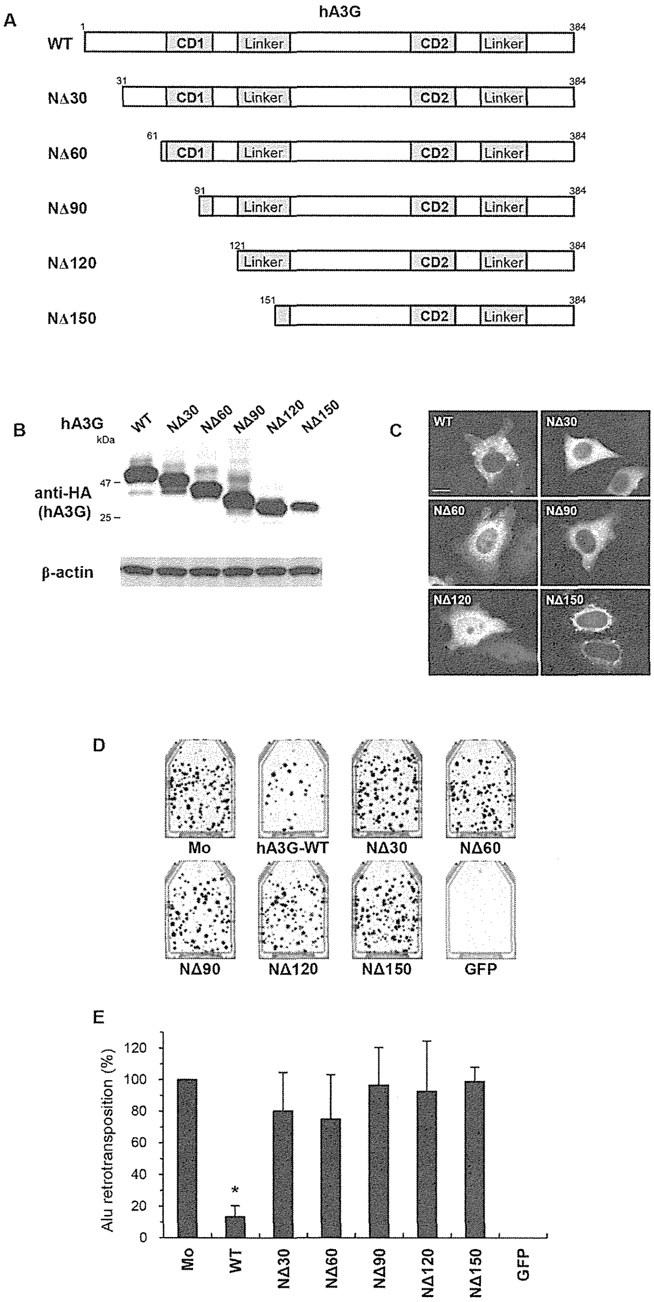

Figure 2. The N-terminal 30 amino acids regulate the anti-Alu activity of hA3G. (**A**) Schematic depiction of a series of N-terminal deletion mutants of hA3G. CD1, N-terminal cytidine deaminase; CD2, C-terminal cytidine deaminase. (**B**) Western blot analysis was performed using extracts from 293T cells transfected with plasmids expressing HA-tagged hA3G mutant proteins. Monoclonal antibodies specific for HA (upper) or β-actin (lower) were used. (**C**) Representative images of HeLa cells transfected with the indicated plasmids are shown. hA3G wild-type (WT), NΔ30, NΔ60, NΔ90, and NΔ120 mutant proteins were predominantly localized to the cytoplasm, whereas NΔ150 mutant protein localized to the perinuclear region. Scale bar: 20 µm. (**D**, **E**) An *Alu* retrotransposition assay was performed as described in Figure 1. Crystal violet-stained G418^R colonies were counted to determine the level of *Alu* retrotransposition. The data shown are the mean ± SD of triplicate experiments. Mo, mock; WT, wild-type hA3G; GFP, GFP only. *P < 0.005, *t*-test.

doi: 10.1371/journal.pone.0084228.g002

Figure 3

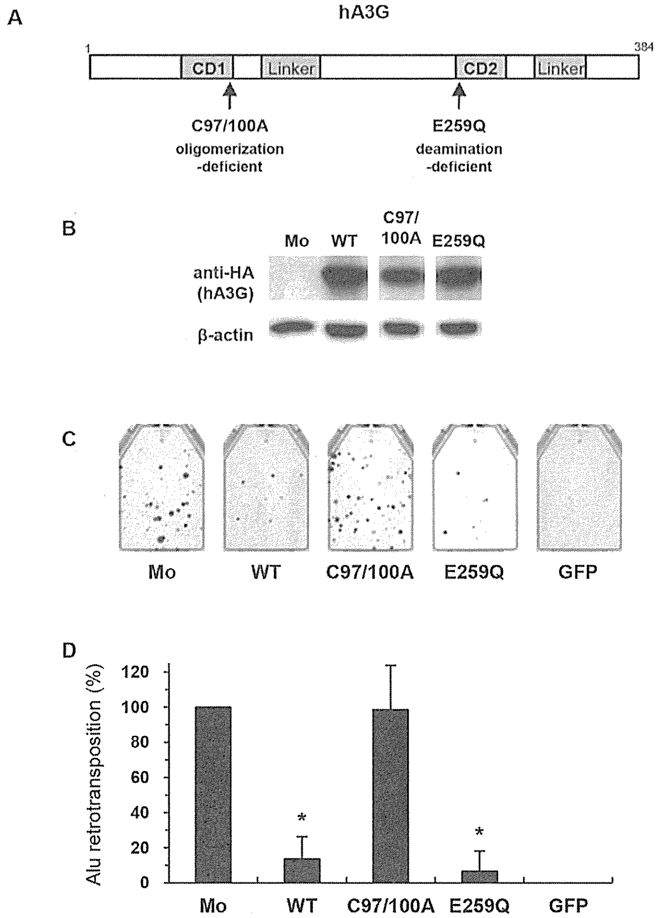

Figure 3. The anti-Alu activity of hA3G is associated with its oligomerization and is independent of its deaminase activity. (**A**) Schematic depiction of two mutants: an oligomerization-deficient mutant, C97/100A, and a deamination-deficient mutant, E259Q. (**B**) Western blot analysis was performed using extracts from 293T cells transfected with plasmids expressing HA-tagged hA3G mutant proteins. Monoclonal antibodies specific for HA (upper) or β-actin (lower) were used. (**C**, **D**) An *Alu* retrotransposition assay was performed as described in Figure 1. A GFP expression vector was used as a negative control. Crystal violet-stained G418^R colonies were counted to determine the level of *Alu* retrotransposition. The data shown are the mean ± SD of triplicate experiments. Mo, mock; WT, wild-type hA3G; GFP, GFP only. **P* < 0.005, *t*-test.

doi: 10.1371/journal.pone.0084228.g003

(Y124, Y125, F126, and W127) that have been predicted to be hot spots of protein–protein interaction [68] and have been reported to be critical for the RNA-mediated oligomerization of hA3G [34,59]. The structural model of hA3G-4G(124–127) indicates that the mutant does not form the aromatic cluster, leaving a prominent space between two monomers (compare

Figure 4

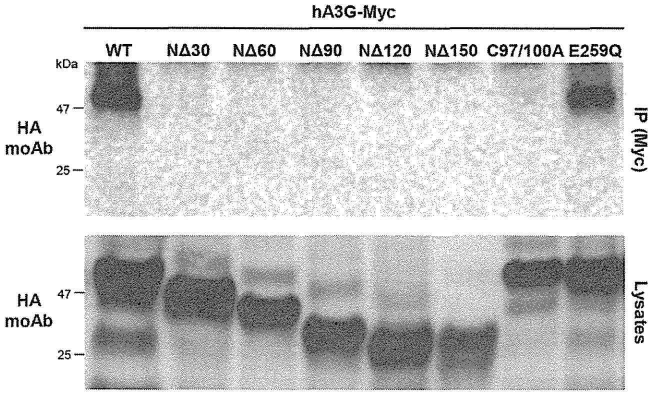

Figure 4. The homooligomerization of hA3G is dependent on the N-terminal 30 amino acid residues of this protein. 293T cells cotransfected with the Myc-tagged and HA-tagged hA3G expression plasmids were immunoprecipitated (IP) with an anti-Myc polyclonal antibody. The resulting complexes were analyzed by immunoblotting with a monoclonal antibody against the HA tag to detect oligomerized hA3G (upper). Cell lysate aliquots were also analyzed in parallel by immunoblotting for the HA tag (lower). WT, wild-type hA3G.

doi: 10.1371/journal.pone.0084228.g004

the left and right panels of Figure 6C and the left and right panels of Figure 6D). Given this result, we then introduced in silico mutations into the five-amino-acid cluster (R24, P25, I26, L27, and S28) of the putative dimer interface (RPILS –> GGGGG; designated 5G(24–28)) (compare the left and right panels of Figure 6E and the left and right panels of Figure 6F). The space between the two monomers of the mutant was clearly comparable to that of 4G(124–127), implying that the 5G(24–28) mutant cannot form a dimer. Based on the structural models, we constructed the myc-tagged N-terminal mutants hA3G-5G(24–28) and hA3G-4G(124–127) to determine whether the former hA3G mutant is unable to physically oligomerize. To assess oligomerization, we performed coimmunoprecipitation-based oligomerization assays using wild-type and mutant hA3G proteins. The 5G(24–28) mutant was not coimmunoprecipitated (Figure 6G), nor was 4G(124–127), suggesting that these mutants do not have the ability to oligomerize. Finally, to determine whether the 4G(124–127) and 5G(24–28) mutants lacks anti-*Alu* activity, we performed the retrotransposition assay and found out that these mutants had completely lost the ability to inhibit *Alu* retrotransposition (Figure 6H). hA3G mutants harboring individual amino acid substitutions (R24G and Y125G) displayed equivalent or moderately less inhibitory activity with comparable dimerization (Figures S3A and S3B). In addition, 5G(24–28) and 4G(124–127) mutations both negatively affect the ability of hA3G to inhibit HIV-1 infection (Figure S4). Taken altogether, these results indicate that the N-terminal amino acid residues 24–28 (RPILS) contribute to the oligomerization of hA3G and its anti-*Alu* retrotransposition activity.

Figure 5

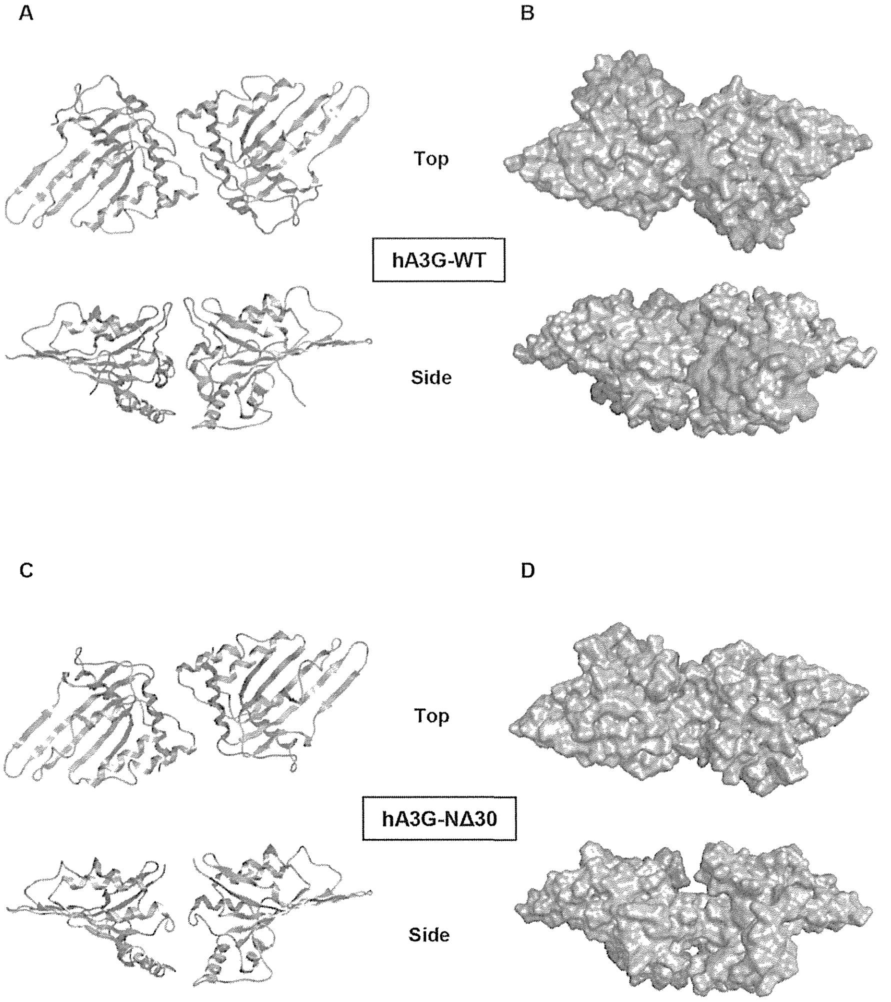

Figure 5. The N-terminal 30 amino acids of hA3G are located at the dimer interface and are therefore key residues for the oligomerization of hA3G. Structural models of the hA3G N-terminal domain. The models were constructed by homology modeling using the X-ray crystal structure of hA2. The head-to-head dimer structure of hA3G N-terminal domain is represented by ribbon models (A and C) and space-filling models (B and D). (**A**, **B**) Views of the top (upper) and side (lower) of wild-type (WT) hA3G. Cyan, N-terminal 30 amino acids of hA3G. (**C**, **D**) Views of the top (upper) and side (lower) of the N-terminal 30-amino-acid deletion mutant of hA3G.

doi: 10.1371/journal.pone.0084228.g005

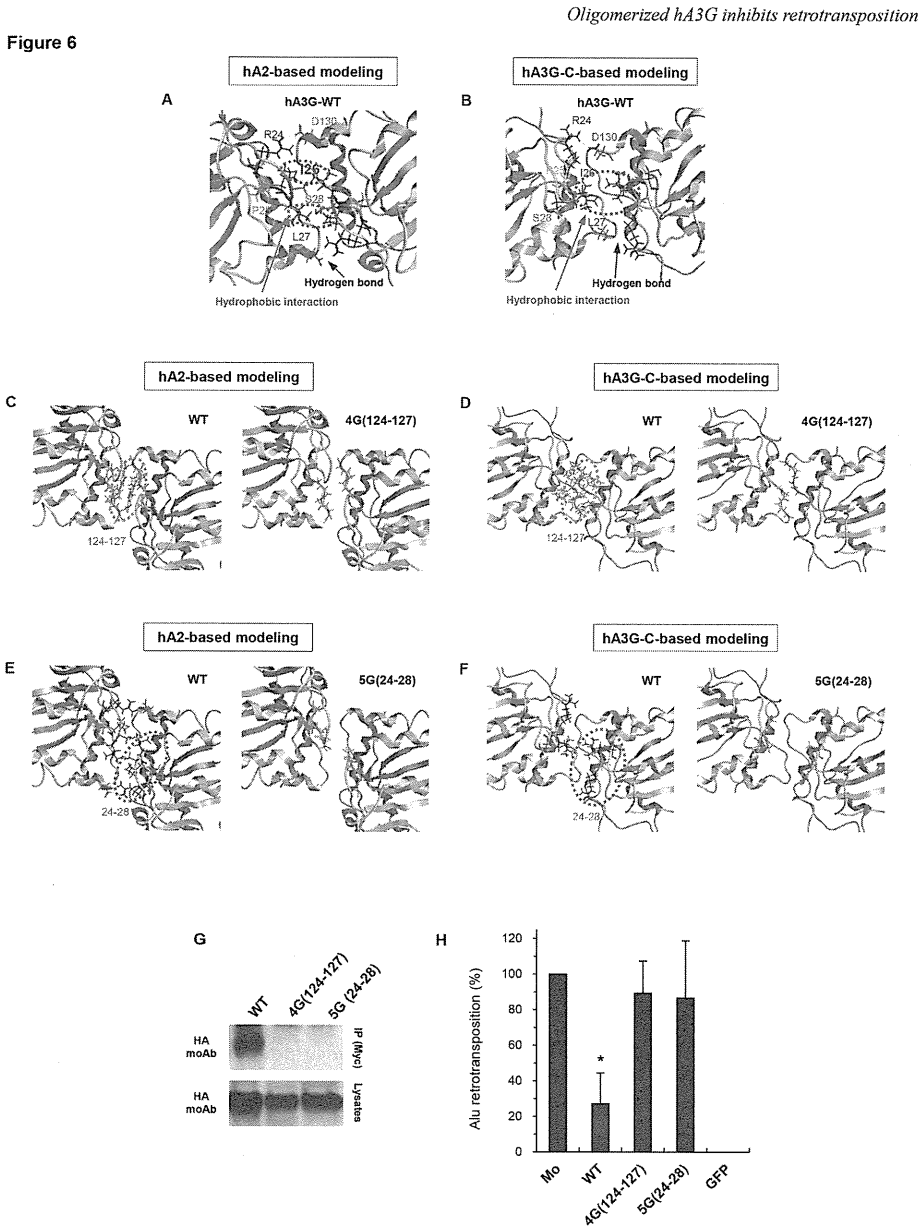

Figure 6. Residues 24–28, as well as known residues 124–127, contribute to the ability of hA3G to homooligomerize and its inhibitory activity against Alu retrotransposition. (A–F) Structural models of hA3G dimer based on the human APOBEC2 (hA2) crystal structure (A, C, and E) and the C-terminal hA3G (hA3G-C) NMR structure (B, D, and F). (**A**, **B**) The interaction surface of the hA3G N-terminal domain in the head-to-head dimer is shown. The hydrophobic interactions formed between either I26 or L27 (green) and their counterpart residues of another monomer (green) are encircled by green dotted lines. A hydrogen bond is formed between a basic residue R24 (blue) and another monomer's D130 (red). Another hydrogen bond is formed between the S28 residues (pink) of two monomers. Structural stability may be conferred by P25 (orange). (**C**, **D**) The dimer interface at amino acid residues 124–127. Left panel, the aromatic amino acid cluster (YYFW) at positions 124–127 is depicted in light green; right panel, the substitution of these residues with glycines is shown in cyan. (**E**, **F**) The dimer interface at amino acid residues 24–28. Left panel, the dimer interface residues (RPILS) at positions 24–28 are depicted in colors similar to those in A; right panel, substitution of these residues with glycines is shown in cyan. (**G**) IP-Western blot analysis was performed as described in Figure 4; upper, IP; lower, cell lysates. (**H**) An *Alu* retrotransposition assay was performed as described in Figure 1. Crystal violet-stained G418R colonies were counted to determine the level of *Alu* retrotransposition. The data shown are the mean ±SD of triplicate experiments. Mo, mock; WT, wild-type hA3G; GFP, GFP only. *P < 0.05, **P < 0.005, t-test.

doi: 10.1371/journal.pone.0084228.g006